

UCSF

UC San Francisco Previously Published Works

Title

Apo States of Calmodulin and CaBP1 Control CaV1 Voltage-Gated Calcium Channel Function through Direct Competition for the IQ Domain

Permalink

<https://escholarship.org/uc/item/9qg6h28s>

Journal

Journal of Molecular Biology, 425(17)

ISSN

0022-2836

Authors

Findeisen, Felix

Rumpf, Christine H

Minor, Daniel L

Publication Date

2013-09-01

DOI

10.1016/j.jmb.2013.06.024

Peer reviewed

Published in final edited form as:

J Mol Biol. 2013 September 9; 425(17): . doi:10.1016/j.jmb.2013.06.024.

Apo-states of calmodulin and CaBP1 control Ca_v1 voltage-gated calcium channel function through direct competition for the IQ domain

Felix Findeisen^{1,3}, Christine Rumpf^{1,3}, and Daniel L. Minor Jr.^{1,2,3,4,*}

¹Cardiovascular Research Institute, University of California, San Francisco, California 94158-2330

²Departments of Biochemistry and Biophysics, and Cellular and Molecular Pharmacology, University of California, San Francisco, California 94158-2330

³California Institute for Quantitative Biomedical Research, University of California, San Francisco, California 94158-2330

⁴Physical Biosciences Science Division, Lawrence Berkeley National Laboratory, Berkeley, CA 94720 USA

Abstract

In neurons, binding of calmodulin (CaM) or calcium-binding protein 1 (CaBP1) to the Ca_v1 (L-type) voltage-gated calcium channel IQ domain endows the channel with diametrically opposed properties. CaM causes calcium-dependent inactivation (CDI) and limits calcium entry, whereas CaBP1 blocks CDI and allows sustained calcium influx. Here, we combine isothermal titration calorimetry (ITC) with cell-based functional measurements and mathematical modeling to show that these calcium sensors behave in a competitive manner that is explained quantitatively by their apo-state binding affinities for the IQ domain. This competition can be completely blocked by covalent tethering of CaM to the channel. Further, we show that Ca²⁺/CaM has a sub-picomolar affinity for the IQ domain that is achieved without drastic alteration of calcium binding properties. The observation that the apo-forms of CaM and CaBP1 compete with each other demonstrates a simple mechanism for direct modulation of Ca_v1 function and suggests a means by which excitable cells may dynamically tune Ca_v activity.

Keywords

Voltage-gated calcium channel; isothermal titration calorimetry; electrophysiology; calcium sensor proteins; mathematical models

Introduction

High-voltage activated calcium channel (Ca_v) opening provides the primary source of calcium influx in excitable cells and couples electrical signals to chemical signaling

© 2013 The Authors. Published by Elsevier Ltd. All rights reserved.

*Correspondence: daniel.minor@ucsf.edu.

Publisher's Disclaimer: This is a PDF file of an unedited manuscript that has been accepted for publication. As a service to our customers we are providing this early version of the manuscript. The manuscript will undergo copyediting, typesetting, and review of the resulting proof before it is published in its final citable form. Please note that during the production process errors may be discovered which could affect the content, and all legal disclaimers that apply to the journal pertain.

cascades^{1; 2}. A set of calcium-dependent autoregulatory mechanisms shape Ca_V activity in response to the influx of the permeant ion^{3; 4} and strongly affect neurotransmitter release, excitation-contraction coupling, and calcium-dependent gene activation^{4; 5}. Crucial among these activity-dependent changes is a process called calcium-dependent inactivation (CDI) that limits calcium entry following channel activation and for which the calcium sensor protein calmodulin is essential^{3; 4; 6; 7}.

Ca_V s are multi-subunit complexes of four main components^{8; 9}: a pore-forming Ca_V1 (L-type) or Ca_V2 (P/Q-, N-, and R-type) Ca_V ₁ subunit¹, a cytoplasmic Ca_V subunit^{10; 11}, the membrane anchored subunit Ca_V ₂¹², and calmodulin (CaM)¹³. In some neurons members of a family of neuronal calcium sensor proteins similar to CaM, known as CaBPs¹⁴ can replace CaM¹⁵. This calcium sensor exchange creates Ca_V s having strikingly different functional properties from those under the control of CaM^{16; 17; 18; 19; 20; 21; 22}. In particular, $\text{Ca}_V1.2$ ^{19; 22; 23} and $\text{Ca}_V1.3$ ^{16; 17} lack CDI when CaBP1, a CaBP highly expressed in the brain and retina¹⁵, is part of the channel complex. CaM and CaBP1 are calcium-binding proteins comprising two lobes that each bear a pair of EF-hands and an interlobe flexible linker^{15; 23; 24}. Structural studies have shown that the calcium-bound forms of the CaM and CaBP1 C-terminal lobes (C-lobes) have similar three-dimensional structures^{23; 24} and compete for binding to the same channel element, the IQ domain²³, whereas the N-terminal lobes (N-lobes) are more divergent²³.

Although multiple Ca_V1 channel segments have been implicated in CaM and CaBP1 function^{25; 26; 27; 28; 29}, the main attachment point for both is the IQ domain of the Ca_V ₁ C-terminal cytoplasmic tail^{6; 17; 19; 25}. Previous studies have shown that CaBP1 and CaM cannot simultaneously bind the $\text{Ca}_V1.2$ IQ domain^{17; 19; 23}; however, evidence for functional competition in the full-length channel has been lacking. Here, we use thermodynamic measurements to investigate the CaM and CaBP1 competition on the $\text{Ca}_V1.2$ IQ domain. Our data show that this competition occurs between apo-states of the respective molecules and that although their IQ domain binding sites overlap, the two calcium sensor proteins bind in different ways. Further, we present experiments using *Xenopus* oocytes that corroborate these biochemical observations and that demonstrate that CaM and CaBP1 can compete directly for control of $\text{Ca}_V1.2$ CDI in living cells. Importantly, mathematical modeling of the CaM-CaBP1 competition based on the ITC measurements predicts the functional competition measured on full-length channels in the context of a cell membrane. This excellent agreement, which emerges from analysis of measurements made in dramatically different milieus, indicates that the simplified biochemical systems investigated here capture the essence of the mechanism by which CaM and CaBP1 competitively alter channel function.

Results

$\text{Ca}^{2+}/\text{CaM}$ has sub-picomolar affinity for the $\text{Ca}_V1.2$ IQ domain

The $\text{Ca}_V1.2$ IQ domain is the main binding site for both $\text{Ca}^{2+}/\text{CaM}$ ^{6; 7} and $\text{Ca}^{2+}/\text{CaBP1}$ ¹⁹. Previous isothermal titration calorimetry (ITC) studies have determined the binding affinities of the individual CaBP1 lobes, N-lobe_{CaBP1} and $\text{Ca}^{2+}/\text{C-lobe}_{\text{CaBP1}}$ ²³, full-length $\text{Ca}^{2+}/\text{CaBP1}$ ²³, and the individual $\text{Ca}^{2+}/\text{CaM}$ lobes, $\text{Ca}^{2+}/\text{N-lobe}_{\text{CaM}}$ and $\text{Ca}^{2+}/\text{C-lobe}_{\text{CaM}}$ ³⁰, for this portion of the $\text{Ca}_V1.2$ C-terminal tail; however, measurement of the affinity of full-length $\text{Ca}^{2+}/\text{CaM}$ for the $\text{Ca}_V1.2$ IQ domain had remained elusive. Hence, we set out to examine this interaction using ITC.

Direct titration of $\text{Ca}^{2+}/\text{CaM}$ into solution containing the $\text{Ca}_V1.2$ IQ domain yielded a complex curve (Fig. 1a) that could not be explained by a single binding event. ITC analysis of $\text{Ca}^{2+}/\text{CaBP1}$ with the $\text{Ca}_V1.2$ IQ domain binding posed similar difficulties that were

surmounted using a displacement titration strategy coupled with thermodynamic cycle analysis²³. Therefore, we tested if a comparable approach would apply here. Indeed, titration of $\text{Ca}^{2+}/\text{CaM}$ into a preformed $\text{Ca}^{2+}/\text{C-lobe}_{\text{CaM}}:\text{Ca}_\text{V}1.2$ IQ domain complex gave a single transition (Fig. 1b). As the affinity of the $\text{Ca}^{2+}/\text{C-lobe}_{\text{CaM}}:\text{Ca}_\text{V}1.2$ IQ binding reaction is known³⁰, we could use a thermodynamic cycle (Fig. 1c) together with competition ligand binding by displacement analysis³¹ to determine the affinity of full-length $\text{Ca}^{2+}/\text{CaM}$ for the $\text{Ca}_\text{V}1.2$ IQ domain. Importantly, there is no detectable interaction between $\text{Ca}^{2+}/\text{CaM}$ and $\text{Ca}^{2+}/\text{C-lobe}_{\text{CaM}}$ that could interfere with the analysis (Fig. 1d).

We find that the affinity of $\text{Ca}^{2+}/\text{CaM}$ for the $\text{Ca}_\text{V}1.2$ IQ domain is exceptionally high, $K_d = 850 \pm 130$ fM, a result that agrees with a previously reported subpicomolar estimate of this interaction³². The affinity of $\text{Ca}^{2+}/\text{CaM}$ for the $\text{Ca}_\text{V}1.2$ IQ domain is ~ 3100 -fold stronger than that of $\text{Ca}^{2+}/\text{C-lobe}_{\text{CaM}}$ (Table 1) and indicates that there is a substantial contribution from the $\text{Ca}^{2+}/\text{N-lobe}_{\text{CaM}}$ that agrees with its extensive $\text{Ca}_\text{V}1.2$ IQ domain contacts^{30; 33}. Although extreme, the sub-picomolar affinity of $\text{Ca}^{2+}/\text{CaM}$ for the $\text{Ca}_\text{V}1.2$ IQ domain is within the bounds other tight $\text{Ca}^{2+}/\text{CaM}:\text{peptide}$ interactions (cf. a calmodulin kinase II peptide, 70 fM)³⁴ but is many orders of magnitude greater than what $\text{Ca}^{2+}/\text{CaM}$ displays for the IQ domain of the distantly related voltage-gated sodium channel $\text{Na}_\text{V}1.5$ (2 μM)³⁵ and the $\text{Na}_\text{V}1.5$ III–IV loop (3 μM)³⁶.

Our previous ITC studies using identical buffer conditions to those used here showed that $\text{Ca}^{2+}/\text{CaBP1}$ binds strongly to the $\text{Ca}_\text{V}1.2$ IQ domain (290 ± 70 pM)²³. Nevertheless, this value is ~ 340 -fold weaker than the $\text{Ca}^{2+}/\text{CaM}:\text{Ca}_\text{V}1.2$ IQ domain interaction. In good agreement with these findings, $\text{Ca}^{2+}/\text{CaBP1}$ was unable to displace $\text{Ca}^{2+}/\text{CaM}$ from a preformed $\text{Ca}^{2+}/\text{CaM}:\text{Ca}_\text{V}1.2$ IQ domain complex (Fig. 1e). This result disagrees with the results reported in pull-down studies of Zhou *et al.*¹⁹; however, the discrepancy is readily explained by the fact that Zhou *et al.*¹⁹ used an $\text{Ca}_\text{V}1.2$ IQ domain construct lacking several key residues that interact with $\text{Ca}^{2+}/\text{CaM}$ including two that bind $\text{Ca}^{2+}/\text{N-lobe}_{\text{CaM}}$ (cf. ³⁰).

Taken together, these ITC experiments establish that $\text{Ca}^{2+}/\text{CaM}$ binds the $\text{Ca}_\text{V}1.2$ IQ domain with an exceptionally high affinity that is several hundred-fold stronger than that of $\text{Ca}^{2+}/\text{CaBP1}$ (Table 1). As the affinity of the individual $\text{Ca}^{2+}/\text{C-lobes}$ differs only three-fold^{23; 30}, the competitive advantage of $\text{Ca}^{2+}/\text{CaM}$ over $\text{Ca}^{2+}/\text{CaBP1}$ for the $\text{Ca}_\text{V}1.2$ IQ domain is almost exclusively due to differences in the contributions from the $\text{Ca}^{2+}/\text{N-lobe}$.

apo-CaBP1 binds the $\text{Ca}_\text{V}1.2$ IQ domain more strongly than apo-CaM

The large affinity differences of $\text{Ca}^{2+}/\text{CaM}$ and $\text{Ca}^{2+}/\text{CaBP1}$ for the $\text{Ca}_\text{V}1.2$ IQ domain preclude effective competition by $\text{Ca}^{2+}/\text{CaBP1}$. However, because $\text{Ca}^{2+}/\text{CaM}$ and $\text{Ca}^{2+}/\text{CaBP1}$ are likely to be present only for brief periods when local calcium levels rise due to channel activity, we reasoned that the physiologically relevant competition for the $\text{Ca}_\text{V}1.2$ IQ domain might occur in the calcium-free, apo-states of the respective calcium sensors. To look for biochemical evidence that could test this idea, we measured the affinities for the $\text{Ca}_\text{V}1.2$ IQ domain of a set of apo-CaM and apo-CaBP1 mimics. In each, we disabled calcium binding through an established strategy in which alanine replaces the first aspartate of the EF-hand consensus sequence^{6; 7; 30}. ‘EF##’ denotes which EF hands carry this change.

Because of limitations on reaching sufficient apo-lobe mimic concentrations for direct titration due to the weak nature of the interaction ($K_d \sim 100$ nM), which would have required concentrations of titrant and target that are not physically well behaved, (~ 500 μM), we derived the apo-CaM lobe ($\text{N-lobe}_{\text{CaM}}\text{EF12}$ and $\text{C-lobe}_{\text{CaM}}\text{EF34}$) and apo-CaBP1 C-lobe ($\text{C-lobe}_{\text{CaBP1}}\text{EF34}$) affinities for the $\text{Ca}_\text{V}1.2$ IQ domain using displacement ITC (Fig. 2a–c) and an analysis similar to Fig. 1c. These experiments showed that loss of calcium

binding capacity in the individual CaM lobes caused a 2–3 order of magnitude affinity reduction relative to the calcium-bound forms: $2,200 \pm 10$ nM versus 2.63 ± 0.07 nM for C-lobe_{CaM}EF34 and Ca^{2+} /C-lobe_{CaM} and >5000 nM versus 57.6 ± 35.5 nM, for N-lobe_{CaM}EF12 and Ca^{2+} :N-lobe_{CaM}, respectively (Figs. 2a and 2b, Table 1). We measured a similar magnitude change for the only CaBP1 lobe that responds to calcium³⁷, C-lobe_{CaBP1}, ($3800 \pm 1,300$ nM versus 10.5 ± 1.9 nM, for C-lobe_{CaBP1}EF34 and Ca^{2+} /C-lobe_{CaBP1}, respectively) (Fig. 2c, Table 1). Thus, the importance of calcium for elevating Ca_v1.2 IQ domain binding affinity is shared among the calcium responsive lobes of both CaM and CaBP1.

We also performed competition ITC experiments using apo-mimics of full length CaM and CaBP1 (CaMEF1234 and CaBP1EF34) (Fig. 2d and e, Table 1). These revealed that in the case of CaM, the large change in affinity for the Ca_v1.2 IQ domain relative to the calcium-bound forms is greatly accentuated in context of the full-length protein, reaching a ~six order of magnitude difference (580 ± 50 nM versus 850 ± 130 fM for CaMEF1234 and Ca^{2+} /CaM, respectively) (Fig. 2d and Table 1). In contrast, the ~300-fold difference for CaBP1 (91 ± 13 nM versus 290 ± 70 pM CaBP1EF34 and Ca^{2+} /CaBP1 Fig. 2e and Table 1) is similar to that of C-lobe_{CaBP1} alone and is consistent with the inability of N-lobe_{CaBP1} to undergo a calcium dependent conformational change²³. The apo-CaM mimic affinity for the Ca_v1.2 IQ domain is close to that reported using in cell fluorescence (1035 nM)³⁸ but in poorer agreement with estimates from *in vitro* fluorescence (~ 50 nM)³⁹. Strikingly, comparison of the apo-state affinities shows that unlike in the calcium-bound states where Ca^{2+} /CaM has a huge advantage over Ca^{2+} /CaBP1, the Ca_v1.2 IQ domain favors binding of apo-CaBP1 by ~7-fold over apo-CaM. Thus, the data suggest that under calcium concentrations that favor the apo-states, CaBP1 could compete effectively with CaM for binding to the Ca_v1.2 IQ domain.

Consequences of CaM-IQ domain affinity for calcium binding

Numerous studies have shown that target engagement can have strong effects on the apparent affinity of CaM for calcium due to thermodynamic linkage^{32; 40; 41}. In this context, the nearly million-fold affinity difference between apo-CaM and Ca^{2+} /CaM for the Ca_v1.2 IQ domain was surprising. As the average affinity of CaM for calcium has been measured to be ~ 15 μM ^{42; 43}, the large differences associated with IQ domain engagement could be taken to suggest that the calcium affinity of IQ domain bound CaM might be shifted into picomolar range. Such a scenario would cause IQ domain bound CaM to remain in the calcium-bound form even at resting levels of intracellular calcium, which are ~ 100 nM^{2; 44}. This would put CaM far outside of the range where it could act as a physiologically relevant sensor for calcium-dependent control of channel function.

To try to understand this situation from a quantitative perspective, we constructed a model to evaluate how the measured large changes in protein-protein interactions might lead to changes in the free energy of calcium binding (Fig. 3a and Appendix 1). This analysis shows that there needs to be only a ~30-fold increase (~ 1.9 kcal mol⁻¹) in the calcium affinity of each CaM EF-hand to account for the ~million-fold (~ 7.7 kcal mol⁻¹) affinity difference measured for the binding of apo-CaM and Ca^{2+} /CaM to the Ca_v1.2 IQ domain. Notably, this relative 30-fold change in Ca^{2+} affinity does not depend on the exact Ca^{2+} affinities of free CaM. This calcium affinity change is in good agreement with experimental estimates based on CaM:Ca_v1.2 IQ association³⁹. The rather modest calcium affinity change arises from the fact that the reaction order is higher than a simple single binding event. The affinities of the four EF-hands of CaM have been determined in a number of studies, e.g. ^{42,45,46}. Taking the values that have been used extensively for modeling studies⁴², e.g. ^{47,48} the affinity change caused by association with the Ca_v1.2 IQ domain, we calculated the fraction of Ca^{2+} ₄:CaM present in both the free and Ca_v1.2 IQ domain-associated forms

(Fig. 3b). Interestingly, the model indicates that the association of CaM with IQ domain shifts the sensitivity of the CaM calcium response from a range of 10–500 μM to 0.3–10 μM . Such a tuning of calcium sensitivity positions the complex perfectly in range of physiologically relevant intracellular calcium changes^{2; 43; 44}.

Consequences of CaBP1-IQ domain affinity for calcium binding

Functional EF hands are not required for CaBP1 to inhibit CDI²³. Nevertheless, given the differences of binding affinity for the Ca_v1.2 IQ domain between apo-CaBP1, and Ca²⁺/CaBP1, which are considerably smaller than those for CaM but are still substantial (Table 1), we performed an equivalent mathematical analysis to consequences of IQ domain binding for the EF-hand affinities for CaBP1 (Appendix 2). This analysis shows that association with the Ca_v1.2 IQ domain alters the affinity of each CaBP1 EF-hand for Ca²⁺ by 18-fold. This relative change in Ca²⁺ affinity upon IQ domain is independent of the absolute Ca²⁺ affinity of free CaBP1. Thus, despite the dramatically smaller change in IQ domain affinity between apo- and Ca²⁺-bound forms of CaBP1 relative to CaM (310 versus 680,000), the fact that there are fewer EF-hands in CaBP1 compared to CaM (2 rather than 4) results in affinity changes for each individual EFhand that are similar for CaBP1 and CaM (18 and 29, respectively). Taking the reported dissociation constants of the individual CaBP1 Ca²⁺ binding sites³⁷, similar to the analysis with CaM, we determined the fraction of the Ca²⁺₂:CaBP1 form of CaBP1 as a function of calcium concentration in both the free and Ca_v1.2 IQ domain-bound forms (Fig. 3d). The reported apparent affinity of free CaBP1 compared for Ca²⁺ is ~10-fold stronger than that of free CaM. Provided that the affinity changes caused by IQ domain binding are distributed equally among the EF-hands, the analysis indicates that this rank order is maintained upon IQ domain binding and that the CaBP1:Ca_v1.2 IQ domain complex will bind Ca²⁺ at lower calcium concentrations than the CaM:Ca_v1.2 IQ domain complex.

CaBP1 and CaM binding sites comprise different Ca_v1.2 IQ domain elements

Previous studies have shown that the Ca²⁺/C-lobes of CaM and CaBP1 have similar structures^{23; 24} and compete for overlapping binding sites on the Ca_v1.2 IQ domain²³. Given the substantial difference in affinities between the calcium-bound forms of full-length CaM and CaBP1 for the Ca_v1.2 IQ domain (Table 1), we were interested in defining the structural basis for these differences. Ca²⁺/CaM engages the Ca_v1.2 IQ domain using a set of six aromatic anchor residues that are divided into two categories based upon the Ca²⁺/CaM lobe they contact³⁰: Ca_v1.2 F1618, F1619 and Y1622 anchor Ca²⁺/N-lobe_{CaM}; Ca_v1.2 Y1627, F1628 and F1631 anchor Ca²⁺/C-lobe_{CaM}. Hence, removal of the Ca²⁺/N-lobe anchors should reduce the affinity of Ca²⁺/CaM for the IQ domain while leaving the affinity for the Ca²⁺/C-lobe_{CaM} unaffected.

To test this idea, we used ITC to determine the affinity of full-length Ca²⁺/CaM and its individual lobes for a mutant of the Ca_v1.2 IQ domain having the three Ca²⁺/N-lobe_{CaM} anchors replaced by alanine (Ca_v1.2 IQ TripleA). In agreement with the predictions from the structure, ITC shows that Ca²⁺/C-lobe_{CaM} binds to Ca_v1.2 IQ TripleA (Fig. 4a) and has an affinity (1.5±0.2 nM, $\Delta G = 0.14 \text{ kcal mol}^{-1}$) and thermodynamic parameters unchanged from wild-type³⁰ (Tables 1 and 2). In contrast, ITC using Ca²⁺/N-lobe_{CaM} (Fig. 4b) revealed an affinity for Ca_v1.2 IQ TripleA that was greatly compromised by the loss of the N-lobe anchors (>5 μM , $\Delta G < -2.7 \text{ kcal mol}^{-1}$) (Tables 1 and 2). In accord with these results, ITC measurements show that the TripleA mutation also reduced the affinity of full-length Ca²⁺/CaM (170±20 pM, $\Delta G = -3 \text{ kcal mol}^{-1}$) for the Ca_v1.2 domain (Fig. 4c and Table 2). Together, these data match expectations set by the structure and underscore the importance of the N-lobe anchors to the overall affinity of Ca²⁺/CaM for the IQ domain.

The Ca²⁺/C-lobe binding sites for CaM and CaBP1 overlap²³ but the detailed differences in the binding modes remain unclear. To test whether the strict separation of aromatic residues into N-lobe and C-lobe anchors also held true for CaBP1, we also measured the effect that the TripleA change had on the affinities of full-length Ca²⁺/CaBP1 and its isolated lobes. In contrast to the results with Ca²⁺/C-lobe_{CaM} (Fig. 4a), the TripleA change lowered the affinity of Ca²⁺/C-lobe_{CaBP1} for the Ca_v1.2 IQ domain by 1.87 kcal mol⁻¹ (Fig. 4d, Table 2), suggesting that at least some of the N-lobe anchors contribute to Ca²⁺/C-lobe_{CaBP1} binding. Similarly, the TripleA change reduced the affinities of both N-lobe_{CaBP1} (>5 μM, $\Delta G < -0.9$ kcal mol⁻¹) (Fig. 4e) and Ca²⁺/CaBP1 (221±14 nM, $\Delta G = 2.04$ kcal mol⁻¹) (Fig. 4f) compared to the wild-type Ca_v1.2 IQ domain²³. The impact of the TripleA change on the affinity of both Ca²⁺/CaBP1 lobes stands in stark contrast to the results with the Ca²⁺/CaM lobes where the affinity of Ca²⁺/N-lobe_{CaM} is reduced but that of Ca²⁺/C-lobe_{CaM} is spared (Fig. 4a). Further, the strong impact on Ca²⁺/C-lobe_{CaBP1}, which has a binding site that overlaps with Ca²⁺/C-lobe_{CaM}²³, indicates that part of the Ca²⁺/C-lobe_{CaBP1} binding site includes some of the N-lobe anchors and provides evidence that the binding determinants for Ca²⁺/CaBP1 and Ca²⁺/CaM interactions with Ca_v1.2 IQ domain are not identical.

Functional competition between CaBP1 and CaM on Ca_v1.2

Given the biochemical evidence that CaM and CaBP1 bind to the Ca_v1.2 IQ domain in a mutually exclusive way (Fig. 1e)^{17; 19; 23}, we wanted to test whether this biochemical competition could be recapitulated in a functional setting. We used two-electrode voltage clamp experiments in *Xenopus* oocytes, a system used previously to study CaBP1 function^{23; 47}, to examine whether increasing CaM expression could overcome the functional effects of CaBP1 on Ca_v1.2. For these studies, we used the Ca_v 2_a subunit so that there would be a negligible contribution to channel inactivation from voltage-dependent inactivation (VDI)²⁸. Thus, under our experimental conditions measurement of Ca_v1.2 inactivation when calcium is the permeant ion yields a direct readout of CDI.

As a first attempt to characterize the competition between CaM and CaBP1, we pursued experiments in which CaBP1 synthesis should happen contemporaneously with that of the channel. Due to endogenous CaM, Ca_v1.2 CDI in oocytes is robust^{6; 23; 30; 48}. We had shown previously that even at a 60:1 excess of CaM:Ca_v1.2 mRNA, CaM expression did not further affect CDI as measured by the fraction of current decrease at 300 milliseconds (t_{i300})⁴⁹. In contrast to these results, changes in CaBP1:Ca_v1.2 mRNA ratios caused clear alterations in t_{i300} and loss of CDI (Fig. 5a and b). Based on these experiments, we chose a 1:1 CaBP1:Ca_v1.2 mRNA ratio as the background for co-injection competition experiments with CaM mRNAs as this ratio achieved nearly full inhibition of CDI ($t_{i300} = 19.3 \pm 5.2\%$) (Fig. 5a and b). Co-injection of 1:1 CaM:CaBP1 mRNA along with the mRNAs for the other channel components resulted in recovery of a small fraction of CDI ($t_{i300} = 28.8 \pm 6.4\%$) (Fig. 5c and d). Increasing the CaM:CaBP1 ratio intensified CDI, which became nearly complete at a ratio of 30:1 CaM:CaBP1 mRNA ($t_{i300} = 52.4 \pm 3.2\%$) (Fig. 5c and d). These experiments support the idea of competitive effects between CaM and CaBP1 for control of CDI.

To test the CaM-CaBP1 competition directly and to exclude factors that might be related to differences in protein synthesis, we examined the effects on Ca_v1.2 CDI resulting from direct injection of purified CaBP1 and CaM protein. The proteins were injected together with 100 mM BAPTA, and thus, should be in the apo-forms and remain so until the local calcium concentration is raised via voltage-dependent Ca_v1.2 activation. Injection of CaBP1 at concentrations of 10 μM or higher into *Xenopus* oocytes expressing Ca_v1.2₁, Ca_v 2_a, and Ca_v 2₋₁ fifteen minutes prior to recording caused unmistakable inhibition of CDI that became nearly complete at 100 μM CaBP1 ($t_{i300} = 6.6 \pm 2.2\%$) (Fig. 6a-c). In contrast,

injection of 0.1 μM or 1 μM CaBP1, or buffer alone had no effect ($t_{i300} = 52.9 \pm 4.7\%$, $56.3 \pm 10.7\%$, and $61.2 \pm 5.4\%$, respectively) (Fig. 6a–c), respectively. This dramatic loss of CDI indicates that the injected CaBP1 competes with endogenous CaM, which is pre-associated with the channel³⁸, for control of CDI.

We next asked whether co-injection of purified CaM together with CaBP1 could antagonize the CDI loss caused by CaBP1. We chose 20 μM CaBP1 as a basis level for these experiments as this concentration was the minimum required to prevent most of CDI ($t_{i300} = 15.3 \pm 3.2\%$) (Fig. 6). We found, in good agreement with the CaM and CaBP1 mRNA co-injection experiments (Fig. 5), that increasing the CaM:CaBP1 protein ratio caused a substantial recovery of CDI. This recovery became near complete when the CaM:CaBP1 ratio reached 50:1 ($t_{i300} = 50.5 \pm 4.9\%$) (Fig. 6d–f). The reciprocal effects of CaBP1 on native CaM (Fig. 6a–c) and co-injected CaM on CaBP1 (Fig. 6d–f) directly demonstrate that there is competition between CaM and CaBP1 in the context of functional Ca_v channels in a live cell membrane. Notably, this competition occurs with either the myristoylated form of CaBP1 (Fig. 5), which causes CaBP1 to localize to membranes⁵⁰, or in the absence of this membrane anchor (Fig. 6).

Tethering CaM to $\text{Ca}_v1.2$ blocks the effects of CaBP1 on CDI

As a final test of the CaM:CaBP1 competition, we investigated the response to direct challenge by CaBP1 of a $\text{Ca}_v1.2$ construct bearing CaM that was covalently tethered to the IQ domain C-terminal end through a glycine-based linker ($\text{Ca}_v1.2\text{-CaM}_T$). This unimolecular construct is similar to one described previously⁵¹ and should raise the CaM effective concentration to at least millimolar with respect to the IQ domain⁵¹. $\text{Ca}_v1.2\text{-CaM}_T$ showed voltage gating and CDI and properties that were similar to wild-type untethered channels, indicating that the tethering did not greatly alter function ($t_{i300} = 54.6 \pm 6.2\%$) (Fig. 7 and Supplementary Fig. S2). However, one property was completely changed. Unlike wild-type channels for which injection of 100 μM CaBP1 prior to recording caused complete inhibition of CDI (Figs. 6a–c and 7a), CaM_T channels were totally resistant to the effects of CaBP1 injection ($t_{i300} = 52.0 \pm 8.2\%$, $P=0.56$ versus $\text{Ca}_v1.2\text{-CaM}_T$ without CaBP1 injection) (Fig. 7b). Because $\text{Ca}_v1.2$ channels bearing a tethered CaM mutant that is incapable of responding to calcium lack CDI⁵¹, we did not pursue competition experiments of such channels with CaBP1 as there would be no functional outcome to measure. Taken together with the protein competition results (Fig. 6 and 7a), the resistance of CaM_T to the functional effects of CaBP1 provides unequivocal support for direct competition on the IQ domain between CaM and CaBP1 for control of CDI.

ITC data predicts functional behavior of the apo-CaM/apo-CaBP1 competition

Although other sites have been implicated in influencing the effects of CaBP1 on channel function^{25; 26; 27; 28; 29}, our studies suggest a simple mechanism in which competition between the apo forms of CaM and CaBP1 on the Ca_v IQ domain cause channels to have or lack CDI, respectively. In order to test this conceptual model in a quantitative manner, we used the ITC-derived affinities of the apo-state and Ca^{2+} -bound forms of CaM and CaBP1 to derive the relationship between the CaM/CaBP1 ratio and the fraction of channels occupied by either the apo- or Ca^{2+} -bound forms of CaM (Appendix 3) (Fig. 8). We then asked whether either curve predicts the competition measured by CDI levels from full-length functioning Ca_v s in living cells. Strikingly, the data from the independently measured CDI values observed from our protein competition experiments (Fig. 6d–e) match exceptionally well with the curve defined by the ITC data for apo-state competition.

Even though there is a remarkably good agreement between the predicted CaM occupancy based on the *in vitro* ITC experiments and the functional competition measured on full-

length channels in the membranes of living cells, other factors might affect the binding constants in the cellular setting. These might include CaM and CaBP1 binding sites located elsewhere on the channel, such as the Ca_v1.2 N-terminal cytoplasmic domain^{22; 27; 47; 52}, or the differences in ionic composition between the *in vitro* ITC experiments and cell interior. To test the sensitivity of the mathematical model to K_d perturbations, we recalculated the relationship between the CaM/CaBP1 ratio and the fraction of channels occupied by either the apo-forms of CaM or CaBP1 in the case in which the K_ds differed from the measured values by a factor of 2 (Fig. 8, teal curves) (i.e. instead of $K_{d_{apoCaBP1}}/K_{d_{apoCaM}} = 7.1$, $K_{d_{apoCaBP1}}/K_{d_{apoCaM}}$ is either 3.55, a 2-fold advantage for CaBP1 relative to the measured values, or 14.2, a 2-fold advantage for CaM) or 10 (Fig. 8, orange curves) (i.e. instead of $K_{d_{apoCaBP1}}/K_{d_{apoCaM}} = 7.1$, $K_{d_{apoCaBP1}}/K_{d_{apoCaM}}$ is either 0.71, a 10-fold advantage for CaBP1, or 71, a 10-fold advantage for CaM). These comparisons clearly show that perturbations as small as ten fold to the K_d in the setting of the cell would greatly disturb the correlation between the measured value and the predicted outcomes. These results strengthen the conclusion that the essence of the functional competition is captured by the reduced system comprising apo-CaM, apo-CaBP1, and the IQ domain and indicate that factors beyond the IQ domain have a minor role, at best, a result that agrees with the recently reported studies from Dascal and colleagues⁵³. Thus, a competition between the Ca²⁺-free forms of CaM and CaBP1 occurring on a single Ca_v1.2 site, the IQ domain, is sufficient to explain the mechanism by which CaBP1 changes Ca_v function.

Discussion

Calcium-dependent inactivation (CDI) is a key negative feedback mechanism that determines how much calcium enters excitable cells following Ca_v voltage-dependent activation^{3; 4; 9; 54}. For Ca_v1.2 and Ca_v1.3 channels in some neurons in the brain and retina, this fundamental property can be altered dramatically by association of CaBP1 rather than CaM with the channel^{16; 17; 19; 22; 55}. This change of calcium sensors has profound consequences for the frequency and duration of the Ca_v generated intracellular calcium signals^{4; 5}, yet the exact mechanism by which this functional alteration occurs has been unclear.

Our studies establish that there is direct competition between the apo-state forms of CaM and CaBP1 for the Ca_v1.2 IQ domain and that this competition controls the ability of the channel to autoregulate through CDI. This competition can be quantitatively explained based on the *in vitro* derived ITC parameters for the interactions of the Ca_v1.2 IQ domain with CaM and CaBP1 (Fig. 8). The exceptionally close agreement between the *in vitro* and cell-based measurements strongly suggests that the biochemical properties of the Ca_v1.2 IQ domain in isolation accurately reflect the biologically relevant function of this portion of the channel. Moreover, perturbations to the K_ds as small as ten-fold eliminate this agreement between prediction and experiment. This behavioral concordance, observed in the very different contexts of an isolated biochemical system and a full-length channel complex in a living cell, is consistent with the apparent structural independence of the Ca_v1.2 IQ domain from other parts of the Ca_v1.2 C-terminal tail^{26; 56}. Interestingly, CaBP4, which is structurally similar to CaBP1²³ and is able to inhibit Ca_v1.3 CDI^{16; 17}, has recently been shown to compete with CaM for the Ca_v1.4 IQ domain and block CDI⁵⁷. These results together with the close conservation of Ca_v1 IQ domain sequences⁸ strongly suggest that the competitive mechanism we define here is generally used by CaBP-Ca_v1 pairs.

Although apo-CaM is thought to be pre-associated with the channel complex through the IQ domain²⁵, the details of this interaction have remained unclear. The excellent agreement we find between the *in vitro* ITC measurements and properties of the apo-CaM:Ca_v1.2 IQ domain interaction measured in living cells provides strong support for the idea that CaM is

associated with the IQ domain under low calcium conditions^{25; 32}. As the IQ domain forms a binding site having an exceptionally high affinity for Ca²⁺/CaM, the pre-positioning of CaM on this channel element suggests that even though its conformation may change, CaM will remain tethered to the IQ domain during the entire gating cycle.

The well documented ability of substrate interactions to change the affinity of CaM for calcium^{32; 40; 41; 43} prompted us to investigate the consequences of the sub-picomolar affinity of the Ca²⁺/CaM:Ca_v1.2 IQ domain complex. Thermodynamic linkage (Fig. 3a) dictates that the very high ratio of binding constants (680,000) between Ca²⁺/CaM and CaM for the Ca_v1.2 IQ domain must increase the calcium affinity of CaM in the IQ domain bound state. Investigation of a thermodynamic model indicates that because of the high order of the reaction, the individual binding constants of each EF hand for calcium do not need to change dramatically (only ~30-fold) in order to compensate for large affinity change in the complex. Hence, a large gain in the protein-protein interaction can be achieved without a change of equivalent magnitude in calcium affinity by virtue of the multiple, coupled calcium binding sites on CaM.

The affinity of isolated CaM for calcium is in the micromolar range⁴², which is outside of the response range of many Ca²⁺/CaM dependent protein complexes⁴³. Association of CaM with the Ca_v1.2 IQ domain tunes the calcium response by ~30-fold into a range, 0.3–10 μM, that allows IQ domain bound CaM to sense calcium concentrations that are much lower than expected based on free CaM and that match well with those expected for intracellular calcium changes^{2; 43; 44}. This situation reinforces a general principle whereby CaM-substrate interactions tune the calcium dependent response of CaM into a physiologically relevant range^{41; 43}. Similar analysis indicates that the reported higher intrinsic affinity of CaBP1 for Ca²⁺ relative to CaM³⁷ combined with the impact of association with the Ca_v1.2 IQ domain yields a complex that has a calcium affinity tuned near the lower limit for intracellular calcium levels^{2; 43; 44}. This result suggests that a CaBP1:Ca_v1.2 IQ domain complex could be responsive to changes in Ca²⁺ levels; however, as prior studies have demonstrated that CaBP1 does not require functional EF hands to inhibit Ca_v1.2 CDI²³, such a response is not central to the ability of CaBP1 to block CDI.

There is a strong structural similarity between the Ca²⁺/C-lobes of CaBP1 and CaM²³. Although previous studies^{17; 19; 23} suggest that the Ca²⁺/CaBP1 and Ca²⁺/CaM binding sites on the IQ domain overlap, the binding modes are thought to differ²³. We show that in contrast to Ca²⁺/CaM binding, which meets the expectations set by the structure of the Ca²⁺/CaM:Ca_v1.2 IQ domain complex³⁰ in which Ca²⁺/N-lobe and Ca²⁺/C-lobe interactions are separated into two sets of aromatic anchors, some determinants of the Ca²⁺/N-lobe_{CaM} site are used by Ca²⁺/C-lobe_{CaBP1}. These observations further support the notion that despite their common Ca²⁺/C-lobe architectures²³, Ca²⁺/CaBP1 engages the Ca_v1.2 IQ domain in a manner that differs from Ca²⁺/CaM.

Our studies establish that there is direct competition between the apo-state forms of CaM and CaBP1 for the Ca_v1.2 IQ domain and that this simple mechanism switches the CDI properties of the channel. The demonstration that CaBP1 or CaM can be chased from channels in live cell membranes with the complementary calcium sensor (Figs. 5, 6, and 8) suggests that such competitive mechanisms may be used *in vivo* for dynamic control of Ca_v function in cells expressing CaBP1, such as hippocampal CA3 neurons¹⁹. In this regard, CaBP1 myristoylation, which localizes CaBP1 to membranes⁵⁰ but is not involved in CDI inhibition²³, could aid the ability of CaBP1 to compete at concentrations lower than those tested here for the non-myristoylated form (Fig. 6). Ca_v1 channels have a privileged role in excitation-transcription coupling^{5; 58}; hence, changes in the net calcium flux caused by substitution of CaM by CaBP1 could induce long-term effects in neuronal function. Finally,

our demonstration that calcium sensors can be exchanged on pre-assembled Ca_v s suggests that this property may enable the introduction of components bearing novel chemical reactivity to probe the conformational changes that underlie CDI.

Materials and Methods

Expression and Purification

Expression and purification of CaBP1_{2–15} and CaM, their individual lobes, and the Ca_v 1.2 IQ domain were as described previously^{23; 30}. The Ca_v 1.2 IQ domain TripleA mutant (Ca_v 1.2 F1618A, F1619A, Y1622A) was purified using the same procedure as for the wild-type Ca_v 1.2 IQ domain^{23; 30}. CaM and CaBP1 lobes with D_A mutations at the first positions of the EF-hand consensus motif indicated were expressed using procedures similar to those used for the wild-type counterparts^{23; 30}. Full-length CaM and CaBP1 with inactivated EF-hands were expressed and purified similarly to the single lobes²³.

Isothermal titration calorimetry

Titration were performed at 15°C using a VP-ITC Microcalorimeter (MicroCal). Samples were dialyzed overnight at 4°C (Slide-A-Lyzer, 2 kDa molecular weight cut-off, Thermo Scientific) against appropriate buffers. Titrations were conducted in 5 mM KCl, 1 mM CaCl_2 , 10 mM Hepes, pH 7.4. After centrifugation at 40,000 rpm for 30 min at 4 °C, protein concentration was determined by absorbance at 280 nm⁵⁹. In cases where precipitation at high concentrations of the syringe component precluded direct titration experiments, such as the EF hand mutants, we used a displacement ITC strategy^{23; 31}. All samples were degassed for 5 minutes prior to loading into the calorimeter. Each ITC experiment consisted of one 4 μ l injection followed by 29 injections of 10 μ l titrant. To correct the baseline either heat of dilution from titrations of injectant into buffer was subtracted or the final titration points were used to estimate the baseline. Data were processed with MicroCal Origin 7.0 using the binding models indicated in the main text.

Electrophysiology

Human Ca_v 1.2 (c1C77, GenBank CAA84346), rat Ca_v 2a (GenBank NP 446303), and Ca_v 2-1 (GenBank NM_00182276), co-expressed with either *Homo sapiens* CaM (GenBank NM_006888) or the short isoform of *Homo sapiens* CaBP1 (GenBank AF169148), which bears a myristoylation site, were used for two-electrode voltage clamp experiments in *Xenopus* oocytes. Details of constructs and two-electrode voltage clamp have been described previously²³. In short, linearized cDNA was translated into capped mRNA using the T7 mMessage kit (Ambion). 50 nl of Ca_v 1, Ca_v 2, Ca_v 2-1, and CaBP1 or CaM mRNA at the molar ratio indicated were injected into stage VI *Xenopus* oocytes. For experiments that involved protein injections into oocytes, equimolar mRNA of Ca_v 1, Ca_v 2, and Ca_v 2-1 were injected 48 hours prior to recording. 15 minutes before recording, 50 nl of a mixture of 0.1M BAPTA and the test proteins at the indicated concentrations were injected. The Ca_v 1.2 tethered CaM construct (Ca_v 1.2-CaM_T) consists of residues 1–1644 of human Ca_v 1.2, followed by a six residue linker (TGGGGG) and residues 1–147 of human CaM. This linker, together with the six disordered residues from the Ca^{2+} 4:CaM N-terminus and Ca_v 1.2 IQ C-terminus³⁰, provides sufficient length to span the required distance in a manner compatible with the structure.

Two-electrode voltage-clamp experiments were performed 2 to 3 days post-injection. Oocytes were injected with 50 nl of 100 mM BAPTA four minutes before recording unless stated otherwise to minimize calcium-activated chloride currents. Recording solutions contained 40 mM $\text{Ca}(\text{NO}_3)_2$, 50 mM NaOH, 1 mM KOH, and 10 mM HEPES, adjusted to pH 7.4 using HNO_3 . Electrodes were filled with 3M KCl and had resistances of 0.3–2.0 M Ω .

CDI was measured using 450 ms depolarizations from a -90 mV holding potential to test potentials of -50 to $+50$ mV in 10 mV steps. Consecutive pulses were separated by 15 s. Leak currents were subtracted using a P/4 protocol. Currents were analyzed with Clampfit 8.2 (Axon Instruments). All results are from at least two independent oocyte batches. The t_{i300} values were calculated from normalized currents at $+20$ mV and represent the percentage inactivation after 300 milliseconds.

Supplementary Material

Refer to Web version on PubMed Central for supplementary material.

Acknowledgments

This work was supported by grants to D.L.M. from NIH R01 HL080050 and the American Heart Association 0740019N. We thank R. Aldrich and M. Grabe for critical comments on the manuscript, and members of the Minor lab for support throughout these studies. D.L.M. is an AHA Established Investigator.

Abbreviations

CaM	calmodulin
Ca²⁺/CaM	Ca ²⁺ ₄ :CaM form of CaM
Ca²⁺/N-lobe_{CaM}	Ca ²⁺ ₂ :N-lobe _{CaM} form of CaM N-terminal lobe
Ca²⁺/C-lobe_{CaM}Ca²⁺₂	C-lobe _{CaM} form of CaM C-terminal lobe
CaBP1	calcium binding protein 1
Ca²⁺/CaBP1	Ca ²⁺ ₂ :CaBP1 form of CaBP1
Ca²⁺/C-lobe_{CaBP1}	Ca ²⁺ ₂ :C-lobe _{CaBP1} form of CaBP1 C-terminal lobe
C-lobe_{CaBP1}EF34 and Ca²⁺/C-lobe_{CaBP1}	CaMEF1234 and CaBP1EF34, apo-mimics of full length CaM and CaBP1, respectively
N-lobe_{CaM}EF12 and C-lobe_{CaM}EF34	individual apo-CaM lobe mimics
C-lobe_{CaBP1}EF34	apo-CaBP1 C-lobe mimic

References

1. Catterall WA. Structure and regulation of voltage-gated Ca²⁺ channels. *Annu Rev Cell Dev Biol.* 2000; 16:521–55. [PubMed: 11031246]
2. Clapham DE. Calcium signaling. *Cell.* 2007; 131:1047–58. [PubMed: 18083096]
3. Dunlap K. Calcium channels are models of self-control. *J Gen Physiol.* 2007; 129:379–83. [PubMed: 17438121]
4. Christel C, Lee A. Ca(2+)-dependent modulation of voltage-gated Ca(2+) channels. *Biochim Biophys Acta.* 2011
5. Wheeler DG, Groth RD, Ma H, Barrett CF, Owen SF, Safa P, Tsien RW. Ca(V)1 and Ca(V)2 channels engage distinct modes of Ca(2+) signaling to control CREB-dependent gene expression. *Cell.* 2012; 149:1112–24. [PubMed: 22632974]
6. Zühlke RD, Pitt GS, Deisseroth K, Tsien RW, Reuter H. Calmodulin supports both inactivation and facilitation of L-type calcium channels. *Nature.* 1999; 399:159–62. [PubMed: 10335846]
7. Peterson BZ, DeMaria CD, Adelman JP, Yue DT. Calmodulin is the Ca²⁺ sensor for Ca²⁺-dependent inactivation of L-type calcium channels. *Neuron.* 1999; 22:549–58. [PubMed: 10197534]
8. Van Petegem F, Minor DL. The structural biology of voltage-gated calcium channel function and regulation. *Biochem Soc Trans.* 2006; 34:887–93. [PubMed: 17052221]

9. Findeisen F, Minor DL Jr. Progress in the structural understanding of voltage-gated calcium channel (CaV) function and modulation. *Channels (Austin)*. 2010; 4:459–74. [PubMed: 21139419]
10. Dolphin AC. beta subunits of voltage-gated calcium channels. *J Bioenerg Biomembr*. 2003; 35:599–620. [PubMed: 15000522]
11. Buraei Z, Yang J. The {beta} Subunit of Voltage-Gated Ca²⁺ Channels. *Physiol Rev*. 2010; 90:1461–506. [PubMed: 20959621]
12. Davies A, Hendrich J, Van Minh AT, Wratten J, Douglas L, Dolphin AC. Functional biology of the alpha(2)delta subunits of voltage-gated calcium channels. *Trends Pharmacol Sci*. 2007; 28:220–8. [PubMed: 17403543]
13. Pitt GS. Calmodulin and CaMKII as molecular switches for cardiac ion channels. *Cardiovasc Res*. 2007; 73:641–7. [PubMed: 17137569]
14. McCue HV, Haynes LP, Burgoyne RD. The diversity of calcium sensor proteins in the regulation of neuronal function. *Cold Spring Harb Perspect Biol*. 2010; 2:a004085. [PubMed: 20668007]
15. Haeseleer F, Sokal I, Verlinde CL, Erdjument-Bromage H, Tempst P, Pronin AN, Benovic JL, Fariss RN, Palczewski K. Five members of a novel Ca(2+)-binding protein (CABP) subfamily with similarity to calmodulin. *J Biol Chem*. 2000; 275:1247–60. [PubMed: 10625670]
16. Cui G, Meyer AC, Calin-Jageman I, Neef J, Haeseleer F, Moser T, Lee A. Ca²⁺-binding proteins tune Ca²⁺-feedback to Cav1.3 channels in mouse auditory hair cells. *J Physiol*. 2007; 585:791–803. [PubMed: 17947313]
17. Yang PS, Alseikhan BA, Hiel H, Grant L, Mori MX, Yang W, Fuchs PA, Yue DT. Switching of Ca²⁺-dependent inactivation of Ca(v)1.3 channels by calcium binding proteins of auditory hair cells. *J Neurosci*. 2006; 26:10677–89. [PubMed: 17050707]
18. Lee A, Westenbroek RE, Haeseleer F, Palczewski K, Scheuer T, Catterall WA. Differential modulation of Ca(v)2.1 channels by calmodulin and Ca²⁺-binding protein 1. *Nat Neurosci*. 2002; 5:210–7. [PubMed: 11865310]
19. Zhou H, Kim SA, Kirk EA, Tippens AL, Sun H, Haeseleer F, Lee A. Ca²⁺-binding protein-1 facilitates and forms a postsynaptic complex with Cav1.2 (L-type) Ca²⁺ channels. *J Neurosci*. 2004; 24:4698–708. [PubMed: 15140941]
20. Few AP, Lautermilch NJ, Westenbroek RE, Scheuer T, Catterall WA. Differential regulation of CaV2.1 channels by calcium-binding protein 1 and visinin-like protein-2 requires N-terminal myristoylation. *J Neurosci*. 2005; 25:7071–80. [PubMed: 16049184]
21. Lautermilch NJ, Few AP, Scheuer T, Catterall WA. Modulation of CaV2.1 channels by the neuronal calcium-binding protein visinin-like protein-2. *J Neurosci*. 2005; 25:7062–70. [PubMed: 16049183]
22. Zhou H, Yu K, McCoy KL, Lee A. Molecular mechanism for divergent regulation of Cav1.2 Ca²⁺ channels by calmodulin and Ca²⁺-binding protein-1. *J Biol Chem*. 2005; 280:29612–9. [PubMed: 15980432]
23. Findeisen F, Minor DL Jr. Structural basis for the differential effects of CaBP1 and calmodulin on Ca(V)1.2 calcium-dependent inactivation. *Structure*. 2010; 18:1617–31. [PubMed: 21134641]
24. Li C, Chan J, Haeseleer F, Mikoshiba K, Palczewski K, Ikura M, Ames JB. Structural insights into Ca²⁺-dependent regulation of inositol 1,4,5-trisphosphate receptors by CaBP1. *J Biol Chem*. 2009; 284:2472–81. [PubMed: 19008222]
25. Erickson MG, Liang H, Mori MX, Yue DT. FRET two-hybrid mapping reveals function and location of L-type Ca²⁺ channel CaM preassociation. *Neuron*. 2003; 39:97–107. [PubMed: 12848935]
26. Kim EY, Rumpf CH, Van Petegem F, Arant RJ, Findeisen F, Cooley ES, Isacoff EY, Minor DL Jr. Multiple C-terminal tail Ca(2+)/CaMs regulate Ca(V)1.2 function but do not mediate channel dimerization. *Embo J*. 2010; 29:3924–38. [PubMed: 20953164]
27. Dick IE, Tadross MR, Liang H, Tay LH, Yang W, Yue DT. A modular switch for spatial Ca²⁺-selectivity in the calmodulin regulation of CaV channels. *Nature*. 2008; 451:830–4. [PubMed: 18235447]
28. Findeisen F, Minor DL Jr. Disruption of the IS6-AID Linker Affects Voltage-gated Calcium Channel Inactivation and Facilitation. *J Gen Physiol*. 2009; 133:327–43. [PubMed: 19237593]

29. Ravindran A, Lao QZ, Harry JB, Abrahami P, Kobrinsky E, Soldatov NM. Calmodulin-dependent gating of Ca(v)1.2 calcium channels in the absence of Ca(v)beta subunits. *Proc Natl Acad Sci U S A*. 2008; 105:8154–9. [PubMed: 18535142]
30. Van Petegem F, Chatelain FC, Minor DL Jr. Insights into voltage-gated calcium channel regulation from the structure of the CaV1.2 IQ domain-Ca2+/calmodulin complex. *Nat Struct Mol Biol*. 2005; 12:1108–15. [PubMed: 16299511]
31. Sigurskjold BW. Exact analysis of competition ligand binding by displacement isothermal titration calorimetry. *Anal Biochem*. 2000; 277:260–6. [PubMed: 10625516]
32. Evans TI, Hell JW, Shea MA. Thermodynamic linkage between calmodulin domains binding calcium and contiguous sites in the C-terminal tail of Ca(V)1.2. *Biophys Chem*. 2011; 159:172–87. [PubMed: 21757287]
33. Fallon JL, Halling DB, Hamilton SL, Quioco FA. Structure of calmodulin bound to the hydrophobic IQ domain of the cardiac Ca(v)1.2 calcium channel. *Structure*. 2005; 13:1881–6. [PubMed: 16338416]
34. Tse JK, Giannetti AM, Bradshaw JM. Thermodynamics of calmodulin trapping by Ca2+/calmodulin-dependent protein kinase II: subpicomolar Kd determined using competition titration calorimetry. *Biochemistry*. 2007; 46:4017–27. [PubMed: 17352496]
35. Sarhan MF, Tung CC, Van Petegem F, Ahern CA. Crystallographic basis for calcium regulation of sodium channels. *Proceedings of the National Academy of Sciences of the United States of America*. 2012; 109:3558–3563. [PubMed: 22331908]
36. Sarhan MF, Van Petegem F, Ahern CA. A Double Tyrosine Motif in the Cardiac Sodium Channel Domain III–IV Linker Couples Calcium-dependent Calmodulin Binding to Inactivation Gating. *Journal of Biological Chemistry*. 2009; 284:33265–33274. [PubMed: 19808664]
37. Wingard JN, Chan J, Bosanac I, Haeseleer F, Palczewski K, Ikura M, Ames JB. Structural analysis of Mg2+ and Ca2+ binding to CaBP1, a neuron-specific regulator of calcium channels. *J Biol Chem*. 2005; 280:37461–70. [PubMed: 16147998]
38. Erickson MG, Alseikhan BA, Peterson BZ, Yue DT. Preassociation of calmodulin with voltage-gated Ca(2+) channels revealed by FRET in single living cells. *Neuron*. 2001; 31:973–85. [PubMed: 11580897]
39. Tang W, Halling DB, Black DJ, Pate P, Zhang JZ, Pedersen S, Altschuld RA, Hamilton SL. Apocalmodulin and Ca2+ calmodulin-binding sites on the CaV1.2 channel. *Biophys J*. 2003; 85:1538–47. [PubMed: 12944271]
40. Milos M, Schaer JJ, Comte M, Cox JA. Microcalorimetric investigation of the interactions in the ternary complex calmodulin-calcium-melittin. *J Biol Chem*. 1987; 262:2746–9. [PubMed: 3818620]
41. Zhang M, Abrams C, Wang LP, Gizzi A, He LP, Lin RH, Chen Y, Loll PJ, Pascal JM, Zhang JF. Structural Basis for Calmodulin as a Dynamic Calcium Sensor. *Structure*. 2012; 20:911–923. [PubMed: 22579256]
42. Linse S, Helmersson A, Forsen S. Calcium binding to calmodulin and its globular domains. *J Biol Chem*. 1991; 266:8050–4. [PubMed: 1902469]
43. Xia Z, Storm DR. The role of calmodulin as a signal integrator for synaptic plasticity. *Nat Rev Neurosci*. 2005; 6:267–76. [PubMed: 15803158]
44. Hille, B. *Ion Channels of Excitable Membranes*. 3. Sinauer Associates, Inc; Sunderland, MA: 2001.
45. Chao LH, Stratton MM, Lee IH, Rosenberg OS, Levitz J, Mandell DJ, Kortemme T, Groves JT, Schulman H, Kuriyan J. A mechanism for tunable autoinhibition in the structure of a human Ca2+/calmodulin-dependent kinase II holoenzyme. *Cell*. 2011; 146:732–45. [PubMed: 21884935]
46. Chiba H, Schneider NS, Matsuoka S, Noma A. A simulation study on the activation of cardiac CaMKII delta-isoform and its regulation by phosphatases. *Biophys J*. 2008; 95:2139–49. [PubMed: 18502812]
47. Oz S, Tsemakhovich V, Christel CJ, Lee A, Dascal N. CaBP1 regulates voltage-dependent inactivation and activation of Ca(V)1.2 (L-type) calcium channels. *J Biol Chem*. 2011; 286:13945–53. [PubMed: 21383011]

48. Ivanina T, Blumenstein Y, Shistik E, Barzilai R, Dascal N. Modulation of L-type Ca²⁺ channels by β gamma and calmodulin via interactions with N and C termini of α 1C. *J Biol Chem.* 2000; 275:39846–54. [PubMed: 10995757]
49. Findeisen F, Tolia A, Arant R, Kim EY, Isacoff E, Minor DL Jr. Calmodulin overexpression does not alter Cav1.2 function or oligomerization state. *Channels (Austin).* 2011; 5:320–4. [PubMed: 21712653]
50. Haynes LP, Tepikin AV, Burgoyne RD. Calcium-binding protein 1 is an inhibitor of agonist-evoked, inositol 1,4,5-trisphosphate-mediated calcium signaling. *J Biol Chem.* 2004; 279:547–55. [PubMed: 14570872]
51. Mori MX, Erickson MG, Yue DT. Functional stoichiometry and local enrichment of calmodulin interacting with Ca²⁺ channels. *Science.* 2004; 304:432–5. [PubMed: 15087548]
52. Benmocha A, Almagor L, Oz S, Hirsch JA, Dascal N. Characterization of the calmodulin-binding site in the N terminus of CaV1.2. *Channels (Austin).* 2009; 3:337–42. [PubMed: 19713738]
53. Oz S, Benmocha A, Sasson Y, Sachyani D, Almagor L, Lee A, Hirsch JA, Dascal N. Competitive and non-competitive regulation of calcium-dependent inactivation in CaV1.2 L-type Ca²⁺ channels by calmodulin and Ca²⁺-binding protein 1. *J Biol Chem.* 2013
54. Halling DB, Aracena-Parks P, Hamilton SL. Regulation of voltage-gated Ca²⁺ channels by calmodulin. *Sci STKE.* 2006; 2006:er1. [PubMed: 16685765]
55. Haeseleer F, Imanishi Y, Maeda T, Possin DE, Maeda A, Lee A, Rieke F, Palczewski K. Essential role of Ca²⁺-binding protein 4, a Cav1.4 channel regulator, in photoreceptor synaptic function. *Nat Neurosci.* 2004; 7:1079–87. [PubMed: 15452577]
56. Fallon JL, Baker MR, Xiong L, Loy RE, Yang G, Dirksen RT, Hamilton SL, Quiocho FA. Crystal structure of dimeric cardiac L-type calcium channel regulatory domains bridged by Ca²⁺* calmodulins. *Proc Natl Acad Sci U S A.* 2009; 106:5135–40. [PubMed: 19279214]
57. Shaltiel L, Pappazios C, Fenske S, Hassan S, Gruner C, Rotzer K, Biel M, Wahl-Schott CA. Complex Regulation of Voltage-dependent Activation and Inactivation Properties of Retinal Voltage-gated Cav1.4 L-type Ca²⁺ Channels by Ca²⁺-binding Protein 4 (CaBP4). *J Biol Chem.* 2012; 287:36312–21. [PubMed: 22936811]
58. Murphy TH, Worley PF, Baraban JM. L-type voltage-sensitive calcium channels mediate synaptic activation of immediate early genes. *Neuron.* 1991; 7:625–35. [PubMed: 1657056]
59. Edelhoch H. Spectroscopic determination of tryptophan and tyrosine in proteins. *Biochemistry.* 1967; 6:1948–54. [PubMed: 6049437]
60. Wang HG, George MS, Kim J, Wang C, Pitt GS. Ca²⁺/calmodulin regulates trafficking of Ca(V)1.2 Ca²⁺ channels in cultured hippocampal neurons. *J Neurosci.* 2007; 27:9086–93. [PubMed: 17715345]

Appendix 1

We modeled the system of CaM, calcium, and the IQ domain using a thermodynamic cycle (Fig. 3a) governed by the following equations:

$$K_1 = ([Ca^{2+}]^4 [CaM]) / [Ca^{2+}_4:CaM] \quad (1)$$

$$K_2 = ([IQ] [CaM]) / [CaM:IQ] \quad (2)$$

$$K_3 = ([IQ] [Ca^{2+}_4:CaM]) / [Ca^{2+}_4:CaM:IQ] \quad (3)$$

$$K_4 = ([Ca^{2+}]^4 [CaM:IQ]) / [Ca^{2+}_4:CaM:IQ] \quad (4)$$

Conservation of free energy dictates that the free energy difference of Ca^{2+} binding is as follows:

$$\Delta\Delta G = \Delta G_2 - \Delta G_3 = \Delta G_1 - \Delta G_4. \quad (5)$$

Consequently, knowing the free energy values of the individual binding reactions for the calcium-bound and calcium-free forms of CaM with the IQ domain, G_2 and G_3 , dictates the difference in calcium affinity (G_{CaM}) for reactions G_1 and G_4 .

The values of G_2 and G_3 are:

$$\Delta G_2 = -8.10 \text{ kcal mol}^{-1} \text{ (Fig. 2 and Table 1)} \quad (6)$$

$$\Delta G_3 = -15.68 \text{ kcal mol}^{-1} \text{ (Fig. 1 and Table 1)} \quad (7)$$

Thus, combining equations (5) with (6) and (7) yields the free energy difference corresponding to:

$$\Delta\Delta G_{\text{CaM}} = \Delta G_1 - \Delta G_4 = 7.58 \text{ kcal mol}^{-1}. \quad (8)$$

G comprises the individual Ca^{2+} affinities of the four EF hands rather than a single binding reaction. Making the simplifying assumption that all CaM EF-hands are affected equally by binding of the IQ domain, results in each EF-hand free energy difference altered by $1.90 \text{ kcal mol}^{-1}$, one fourth of the total free energy difference of $7.58 \text{ kcal mol}^{-1}$, at 288K, an increase of 28.8 fold in the calcium affinity of each individual EF-hand. Although the CaM EF-hands may not be affected equally, in the context of the limits set by the thermodynamic cycle (Fig. 3a) any unequal changes in EF-hand affinity would result in only modest changes in relation shown in Fig. 3b.

Appendix 2

We modeled the system of CaBP1, calcium, and the IQ domain using a thermodynamic cycle (Supplementary Figure S1), using an equivalent analysis to that presented in Appendix 1 for CaM as follows:

$$K_1 = ([\text{Ca}^{2+}]^2 [\text{CaBP1}]) / [\text{Ca}^{2+}_2 : \text{CaBP1}] \quad (9)$$

$$K_2 = ([\text{IQ}] [\text{CaBP1}]) / [\text{CaBP1} : \text{IQ}] \quad (10)$$

$$K_3 = ([\text{IQ}] [\text{Ca}^{2+}_2 : \text{CaBP1}]) / [\text{Ca}^{2+}_2 : \text{CaBP1} : \text{IQ}] \quad (11)$$

$$K_4 = ([\text{Ca}^{2+}]^2 [\text{CaBP1} : \text{IQ}]) / [\text{Ca}^{2+}_2 : \text{CaBP1} : \text{IQ}] \quad (12)$$

For CaBP1, the values of G_2 and G_3 are:

$$\Delta G_2 = -9.15 \text{ kcal mol}^{-1} \text{ (Table 1 and Figure 2)} \quad (13)$$

$$\Delta G_3 = -12.38 \text{ kcal mol}^{-1} \text{ (Table 1 and ref. } 23) \quad (14)$$

Thus, combining equations (5) with (18) and (19) yields an difference of free energy corresponding to:

$$\Delta \Delta G_{\text{CaBP1}} = \Delta G_1 - \Delta G_4 = 3.23 \text{ kcal mol}^{-1} \quad (15)$$

Making the simplifying assumption that both functional CaBP1 EF-hands are affected equally by binding of the IQ domain specifies that each EF-hand free energy difference altered by $1.62 \text{ kcal mol}^{-1}$, half of $3.23 \text{ kcal mol}^{-1}$, equivalent to an increase of 17.5 fold in the calcium affinity of each individual EF-hand.

Appendix 3

The ITC data (Figure 1 and Table 1) dictates the following relationships for the calcium-bound forms of CaM and CaBP1:

$$K_{\text{dCaM}} = [\text{IQ}] [\text{CaM}] / [\text{CaM:IQ}] = 850 \text{ fM} \quad (27)$$

and

$$K_{\text{dCaBP1}} = [\text{IQ}] [\text{CaBP1}] / [\text{CaBP1:IQ}] = 290 \text{ pM} \quad (28)$$

Dividing (27) by (28) gives:

$$K_{\text{dCaM}} / K_{\text{dCaBP1}} = [\text{CaM}] [\text{CaBP1:IQ}] / [\text{CaM:IQ}] [\text{CaBP1}] = 0.0029 \quad (29)$$

Rearranging this equation to yield the ratio between the IQ domains occupied by the two Ca^{2+} sensors yields:

$$[\text{CaM}] / [\text{CaBP1}] = 0.0029 [\text{CaM:IQ}] / [\text{CaBP1:IQ}] \quad (30)$$

which can be solved for any given ratio of calmodulin and CaBP1.

We assume that competition between CaBP1 and CaM occurs exclusively on the $\text{Ca}_v1.2$ IQ domain, allowing us to substitute the full-length channel for the IQ domain.

$$[\text{CaM:Ca}_v1.2] / [\text{CaBP1:Ca}_v1.2] = 0.0029 [\text{CaM}] / [\text{CaBP1}] \quad (31)$$

This assumption ignores the possible influence of other sites on $\text{Ca}_v1.2$ that have been shown to have affinity for both CaM^{25; 27} and CaBP1^{19; 22}. Notably, such sites have a >5-fold weaker affinity than the $\text{Ca}_v1.2$ IQ domain for CaM^{32; 52}.

We furthermore assume that there is always one calcium sensor bound to the $\text{Ca}_v1.2$ IQ domain, i.e.

$$[\text{Ca}_v1.2]_{\text{total}} = [\text{CaBP1:Ca}_v1.2] + [\text{CaM:Ca}_v1.2] \quad (32)$$

For (32), given that without CaM, Ca_v1.2 trafficking to the plasma membrane is heavily compromised⁶⁰, we assume that the amount of Ca_v1.2 the plasma membrane of the test *Xenopus* oocyte lacking either calcium sensor is negligible.

Similar analysis for the apo state values (Figure 2 and Table 1) yields the following equations:

$$[\text{CaMEF1234}]/[\text{CaBP1EF34}] = 7.1 [\text{CaBP1EF34}/\text{IQ}]/[\text{CaMEF1234}/\text{IQ}] \quad (33)$$

and

$$[\text{CaMEF1234}]/[\text{CaBP1EF34}] = 7.1 [\text{CaBP1EF34}:\text{Ca}_{\text{v}}1.2]/[\text{CaMEF1234}:\text{Ca}_{\text{v}}1.2] \quad (34)$$

Equations (31) and (34) can be used to derive the relationship between the CaM/CaBP1 ratio and the fraction of the channel occupied by CaM in high (Fig. 8, grey curve) and low Ca²⁺ (Fig. 8, black curve).

- Calmodulin (CaM) and CaBP1 differentially control voltage-gated calcium channels
- CaM and CaBP1 apo-state competition on the Ca_v IQ domain directly controls function
- *In vitro* binding constants predict apo-CaM/apo-CaBP1 competition in live cells
- Ca²⁺/CaM has a sub-picomolar affinity for the IQ domain
- Exchange of apo-CaM and apo-CaBP1 provides dynamic modulation of channel behavior

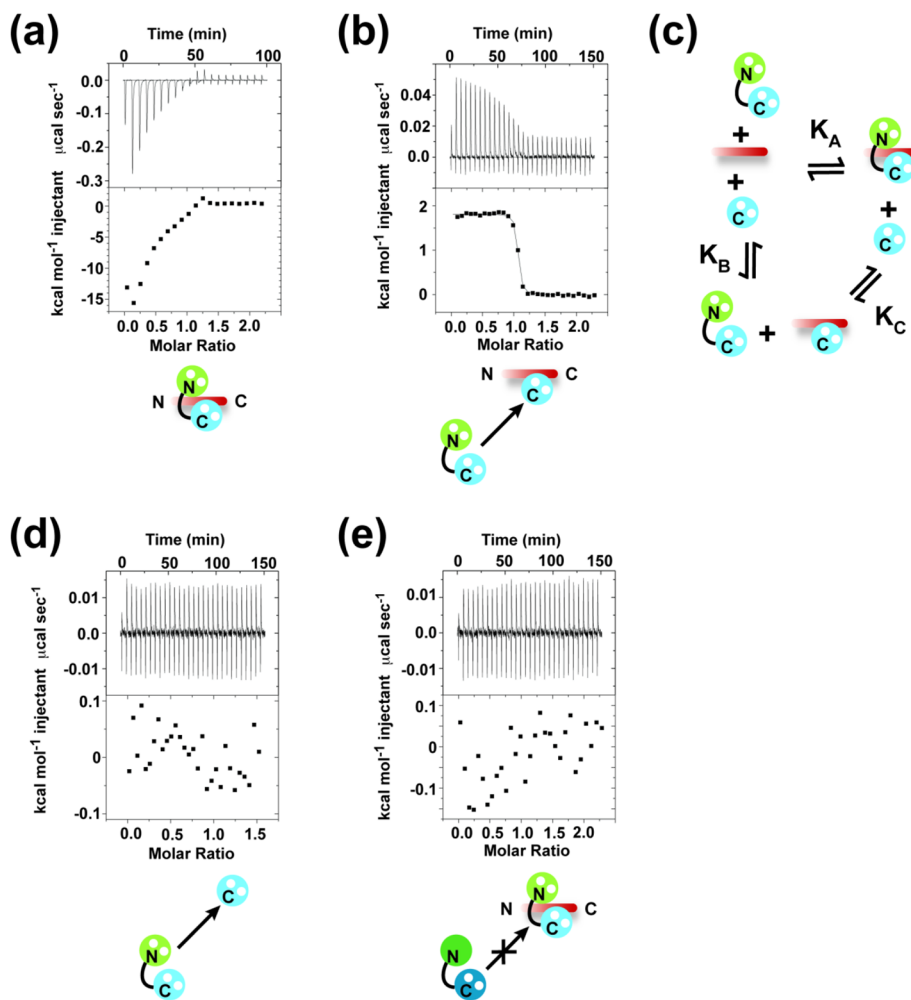


Fig. 1. Characterization of $\text{Ca}^{2+}_4:\text{CaM}-\text{Ca}\gamma 1.2$ IQ domain binding
 Exemplar ITC titrations for: **a**, $75 \mu\text{M}$ $\text{Ca}^{2+}_4:\text{CaM}$ into $7.5 \mu\text{M}$ $\text{Ca}\gamma 1.2$ IQ domain and **b**, $75 \mu\text{M}$ $\text{Ca}^{2+}_4:\text{CaM}$ into $7.5 \mu\text{M}$ $\text{Ca}\gamma 1.2$ IQ domain and $50 \mu\text{M}$ $\text{Ca}^{2+}_2:\text{C-lobe}_{\text{CaM}}$. **c**, Thermodynamic cycle for analysis of the binding of $\text{Ca}^{2+}_4:\text{CaM}$ (K_A) to the $\text{Ca}\gamma 1.2$ IQ domain. K_B describes $\text{Ca}^{2+}_2:\text{C-lobe}_{\text{CaM}}$ binding. K_C describes the competition of $\text{Ca}^{2+}_2:\text{C-lobe}_{\text{CaM}}$ by CaM . Exemplar ITC titrations for: **d**, $75 \mu\text{M}$ $\text{Ca}^{2+}_4:\text{CaM}$ into $50 \mu\text{M}$ $\text{Ca}^{2+}_2:\text{C-lobe}_{\text{CaM}}$ and **e**, $75 \mu\text{M}$ $\text{Ca}^{2+}_2:\text{CaBP1}$ into $7.5 \mu\text{M}$ $\text{Ca}\gamma 1.2$ IQ domain and $11.25 \mu\text{M}$ $\text{Ca}^{2+}_4:\text{CaM}$. Icons depict ITC components. N-lobes and C-lobes are green and blue, respectively. CaM and CaBP1 are in pastel and dark shades, respectively. White spheres represent Ca^{2+} . $\text{Ca}\gamma 1.2$ IQ domain is shown in red.

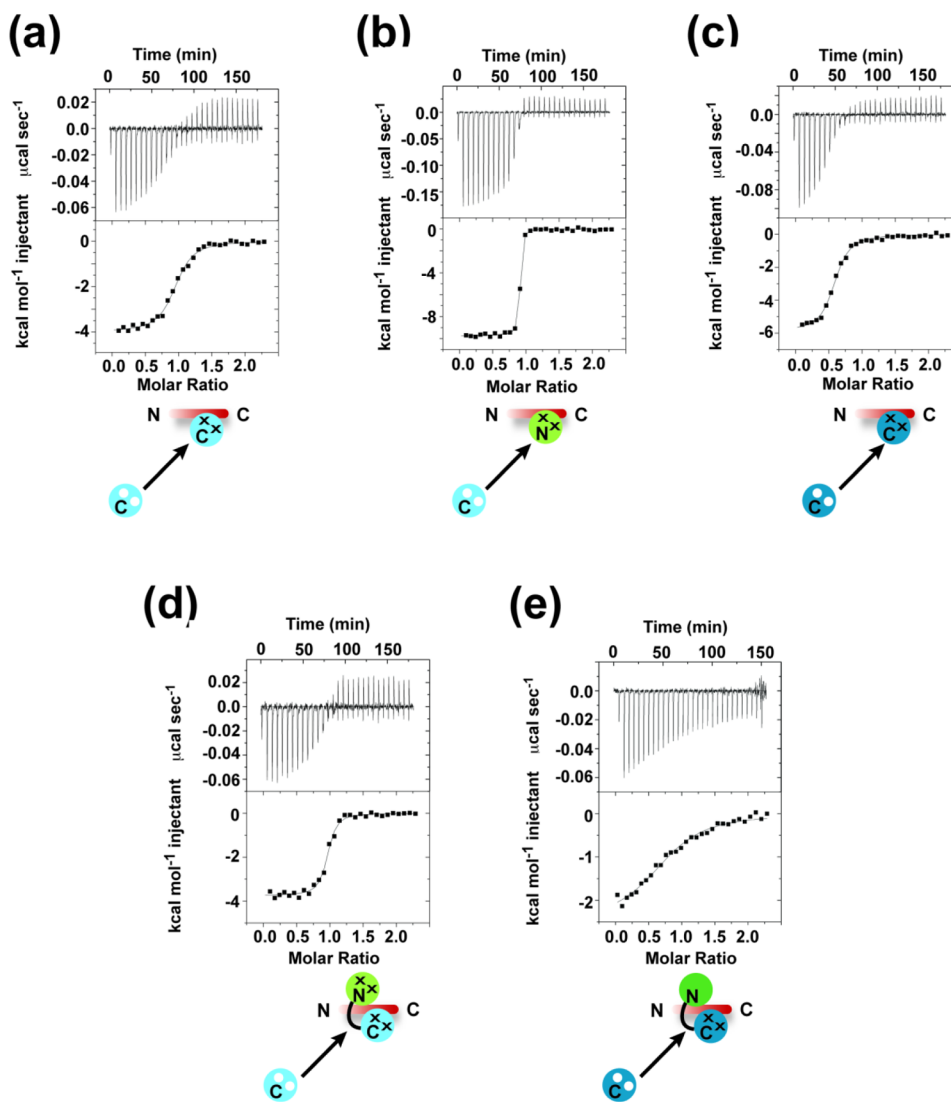


Fig. 2. Characterization of apo-CaM and apo-CaBP1 Ca_V1.2 IQ domain binding

Exemplar ITC titrations for: **a**, 75 μM Ca²⁺₂: C-lobe_{CaM} into 7.5 μM Ca_V1.2 IQ domain and 50 μM C-lobe_{CaM} EF34. **b**, 75 μM Ca²⁺₂: C-lobe_{CaM} into 7.5 μM Ca_V1.2 IQ domain and 50 μM N-lobe_{CaM}EF12. **c**, 75 μM Ca²⁺₂: C-lobe_{CaBP1} into 7.5 μM Ca_V1.2 IQ domain and 50 μM C-lobe_{CaBP1}EF34. **d**, 75 μM Ca²⁺₂: C-lobe_{CaM} into 7.5 μM Ca_V1.2 IQ domain and 50 μM CaMEF1234. **e**, 75 μM Ca²⁺₂: C-lobe_{CaBP1} into 7.5 μM IQ domain and 50 μM CaBP1EF34. Icons depict ITC components. N-lobes and C-lobes are green and blue, respectively. CaM and CaBP1 are in pastel and dark shades, respectively. White spheres represent Ca²⁺. Black crosses indicate mutated EF-hands. Ca_V1.2 IQ domain is shown in red.

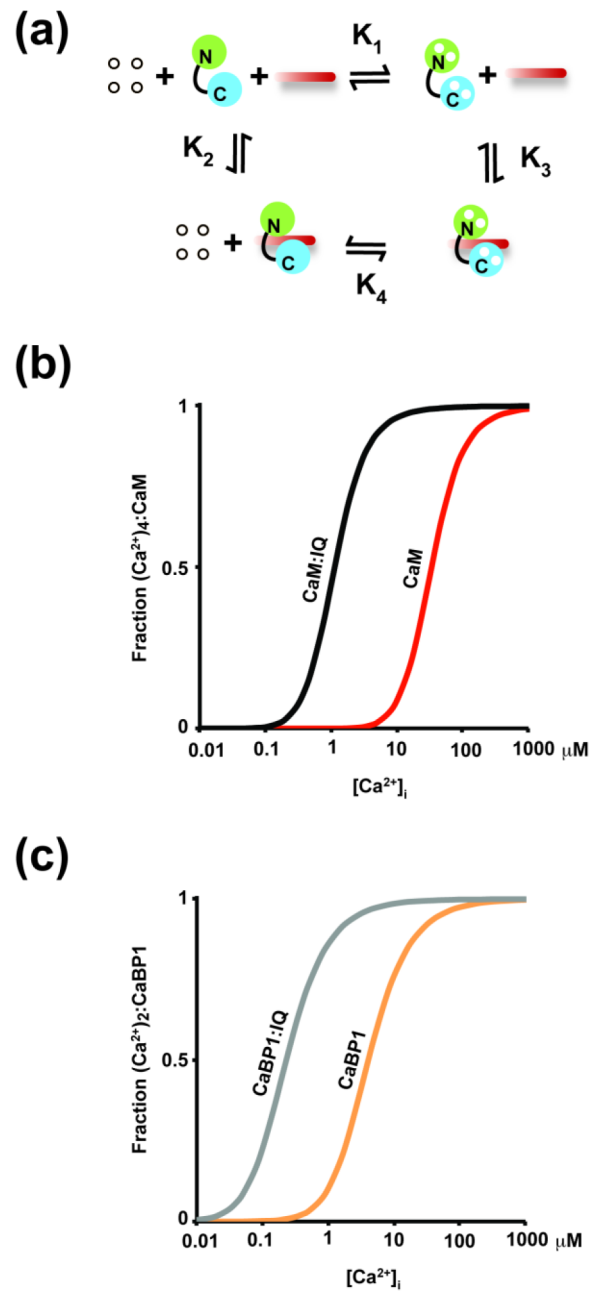


Fig. 3. Thermodynamic analysis of CaM, Ca²⁺, and IQ domain binding
a, Macroscopic thermodynamic cycle for CaM, Ca²⁺ and Ca_v1.2 IQ domain. K₁ and K₄ describe Ca²⁺ binding to CaM and the CaM/IQ complex, respectively. K₂ and K₃ describe IQ domain binding to calcium-free CaM and Ca²⁺₄:CaM, respectively. **b**, Calculated fraction of Ca²⁺₄:CaM as a function of Ca²⁺ concentration for CaM alone (red) or bound to the IQ domain (black curve). **c**, Macroscopic thermodynamic cycle for CaBP1, Ca²⁺ and Ca_v1.2 IQ domain. K₁ and K₄ describe Ca²⁺ binding to CaBP1 and the CaBP1/IQ complex, respectively. K₂ and K₃ describe IQ domain binding to calcium-free CaBP1 and Ca²⁺₂:CaBP1, respectively. **d**, Calculated fraction of Ca²⁺₂:CaBP1 as a function of Ca²⁺ concentration for CaBP1 alone (orange) or bound to the IQ domain (grey curve).

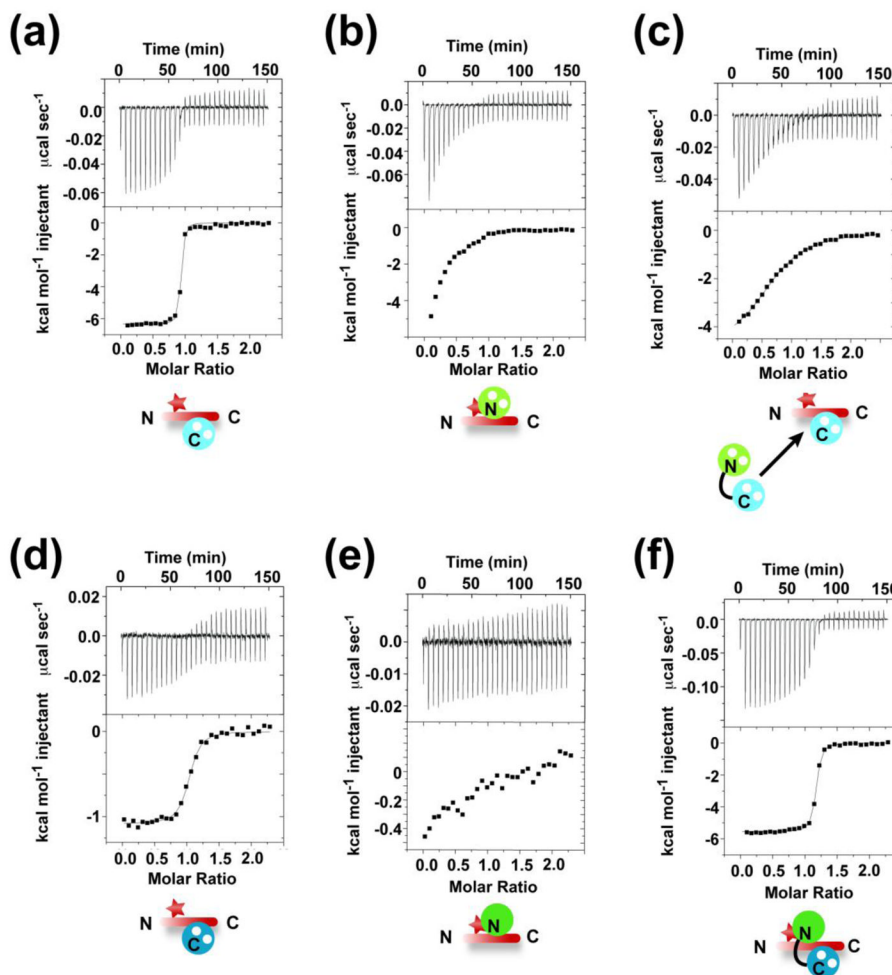


Fig. 4. Characterization of CaM and CaBP1 binding to the Cav1.2 IQ domain mutant ‘TripleA’
 Exemplar ITC titrations for: **a**, 75 μM Ca^{2+}_2 :C-lobe_{CaM} into 7.5 μM TripleA. **b**, 75 μM Ca^{2+}_2 :N-lobe_{CaM} into 7.5 μM TripleA. **c**, 75 μM Ca^{2+}_4 :CaM into 7.5 μM TripleA and 50 μM Ca^{2+}_2 :C-lobe_{CaM}. **d**, 75 μM Ca^{2+}_2 :C-lobe_{CaBP1} into 7.5 μM TripleA. **e**, 75 μM Ca^{2+}_2 :CaBP1 into 7.5 μM TripleA. **f**, 75 μM Ca^{2+}_2 :N-lobe_{CaM} into 7.5 μM TripleA. Icons depict ITC components. N-lobes and C-lobes are green and blue, respectively. CaM and CaBP1 are in pastel and dark shades, respectively. White spheres represent Ca^{2+} . Cav1.2 IQ domain is shown in red. Red star signifies the TripleA mutation.

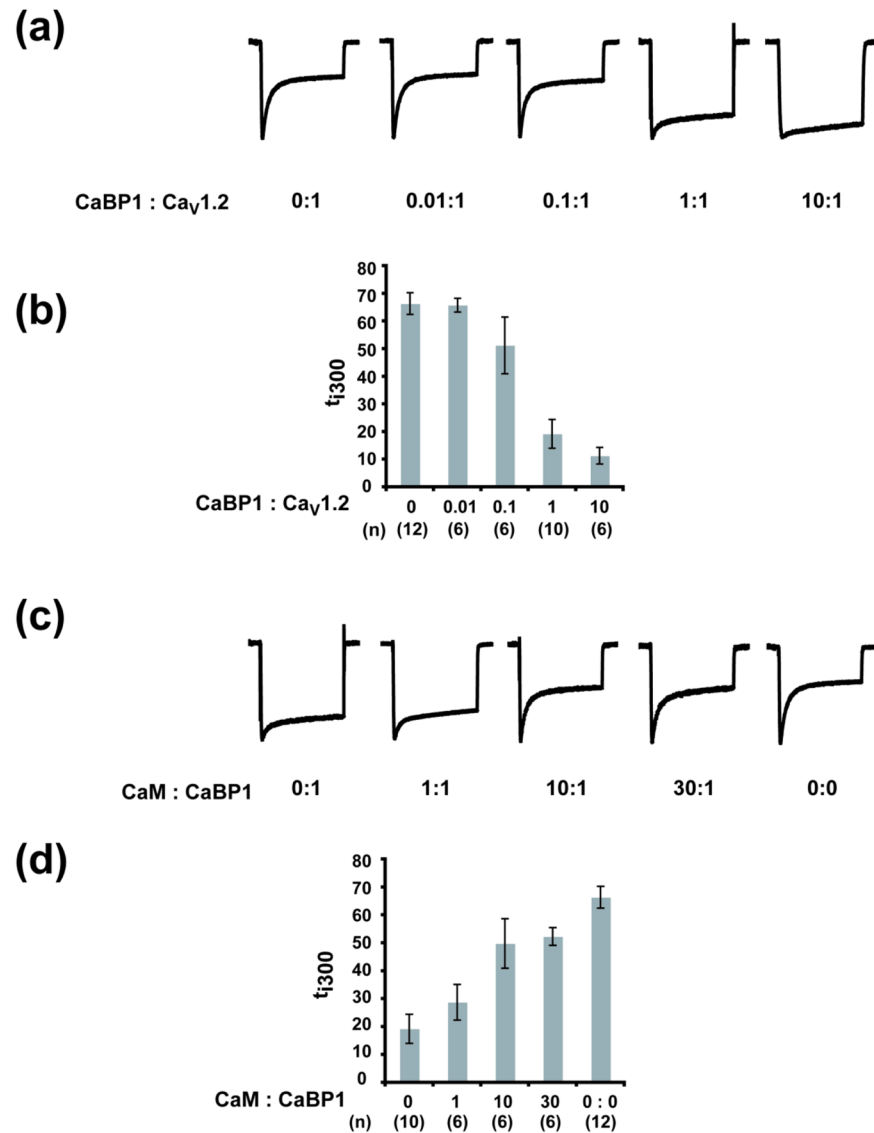


Fig. 5. CaBP1 and CaM expressed in *Xenopus* oocytes compete for control of $Ca_V1.2$ function
a, Representative normalized I_{Ca} traces at a test potential of +20 mV for *Xenopus* oocytes co-expressing $Ca_V1.2$ and CaBP1 at the indicated ratios. **b**, Averaged t_{300} values from normalized I_{Ca} traces at a test potential of +20 mV for $Ca_V1.2$ expressed with CaBP1 at the indicated ratios. (n) indicates the number of experiments. **c**, Representative normalized I_{Ca} traces at a test potential of +20 mV for *Xenopus* oocytes co-expressing $Ca_V1.2$ and the indicated ratios of CaBP1 and CaM. **d**, Averaged t_{300} values from normalized I_{Ca} traces at a test potential of +20 mV for $Ca_V1.2$ expressed with CaBP1 and CaM at the indicated ratio. In all experiments RNA for Ca_V2a and Ca_V2-1 was injected at concentrations equimolar to $Ca_V1.2$. (n) indicates the number of experiments. Trace for 1:1 CaBP1: $Ca_V1.2$ in panel **a** and its corresponding analysis in panel **b** are reproduced in panels **c** and **d** and labeled CaM : CaBP1 0:1.

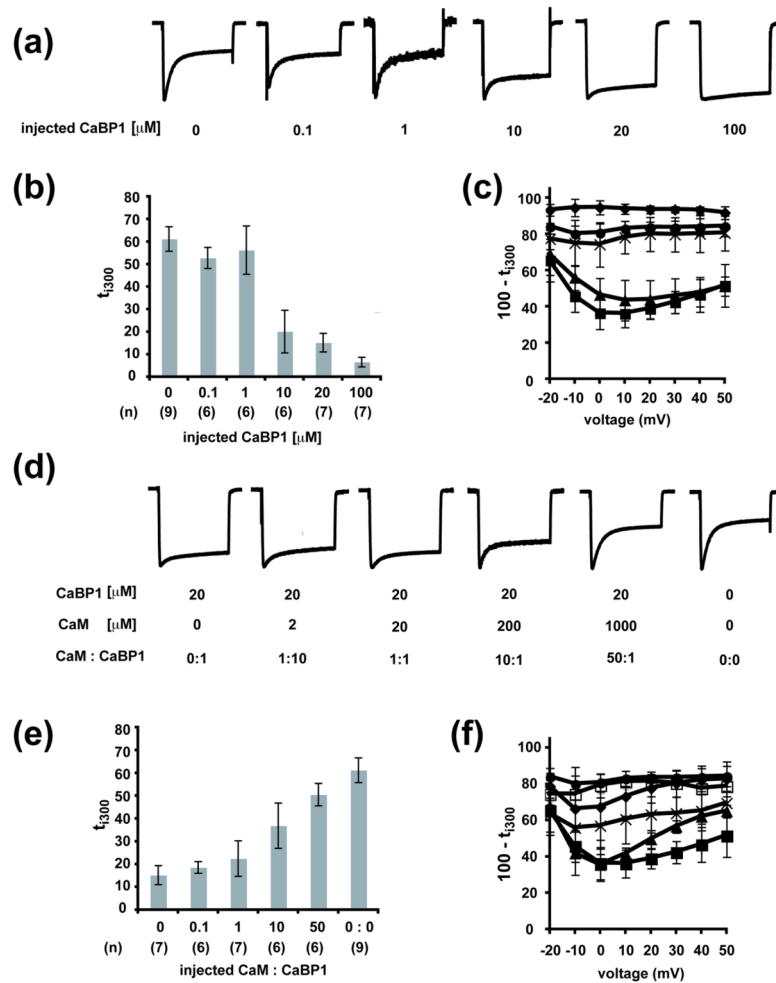


Fig. 6. Purified CaBP1 and CaM injected into cells expressing Ca v 1.2 compete for control of channel function
a, Representative normalized I_{Ca} traces at a test potential of +20 mV for *Xenopus* oocytes expressing Ca v 1.2 and injected with 50 nl of the indicated concentrations of purified CaBP1 15 minutes prior to recording. **b**, Averaged t_{300} from normalized I_{Ca} traces at a test potential of +20 mV from *Xenopus* oocytes expressing Ca v 1.2 injected with 50 nl CaBP1 protein at the indicated concentration 15 minutes prior to recording. (n) indicates the number of experiments. **c**, Voltage-dependence of the averaged normalized current 300 ms after channel activation ($100 - t_{300}$) from oocytes expressing Ca v 1.2 and injected with purified CaBP1 at the following concentrations prior to recording: 0 μ M, \square ; 1 μ M, \circ ; 10 μ M, \triangle ; 20 μ M, \square ; 100 μ M, \bullet . **d**, Representative normalized I_{Ca} traces at a test potential of +20 mV for *Xenopus* oocytes expressing Ca v 1.2 co-injected with the indicated concentrations of purified CaBP1 and CaM. **e**, Averaged t_{300} from normalized I_{Ca} traces at a test potential of +20 mV from oocytes expressing Ca v 1.2 and injected with purified CaM and CaBP1 at the indicated ratios. (n) indicates the number of experiments. **f**, Voltage-dependence of the averaged normalized current 300 ms after channel activation ($100 - t_{300}$) from *Xenopus* oocytes expressing Ca v 1.2 and injected with purified CaM and CaBP1 1 at the following concentrations prior to recording: no CaM or CaBP1, \square ; 20 μ M CaBP1 only, \circ ; 20 μ M CaBP1 and 2 μ M CaM, \triangle ; 20 μ M CaBP1 and 20 μ M CaM, \square ; 20 μ M CaBP1 and 200 μ M CaM, \bullet ; 20 μ M CaBP1 and 1 mM CaM, \circ . 20 μ M CaBP1 trace in panel **a** and its

corresponding analysis in panels in **b** and **c** are reproduced in panels **d**, **e**, and **f** and labeled as 0 μM CaM.

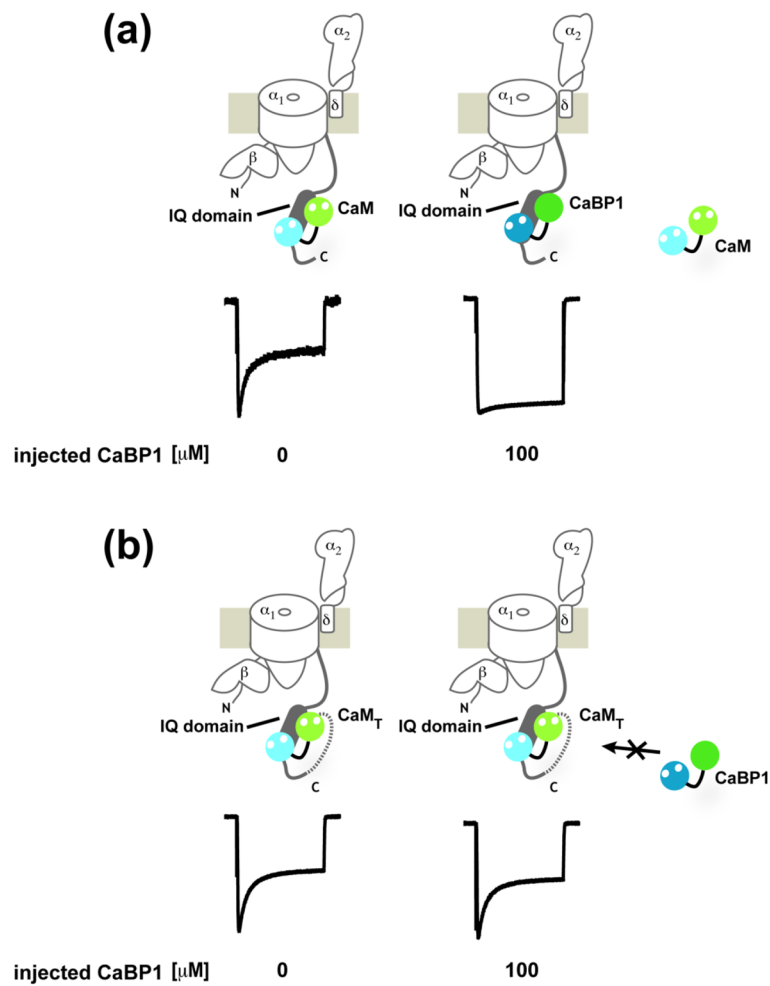


Fig. 7. Ca_v1.2-CaM_T channel CDI resists CaBP1 inhibition
a, Exemplar traces of Ca_v1.2 with and without saturating amounts of CaBP1. The diagrams indicate Ca²⁺ channel subunits, CaM and CaBP1. **b**, Exemplar traces of Ca_v1.2-CaM_T with the same amounts of CaBP1 as in 'a'.

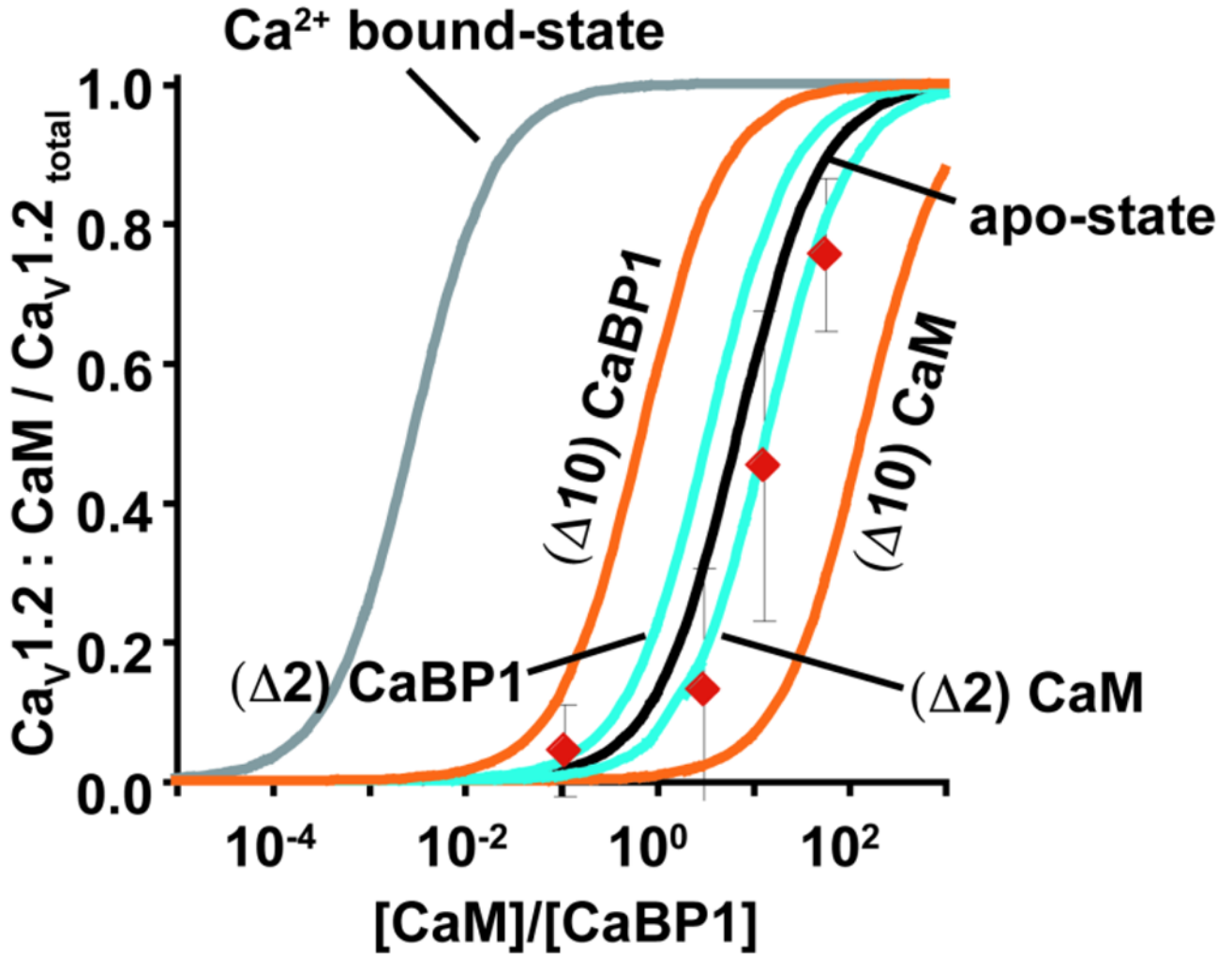


Fig. 8. Functional outcomes of CaM/CaBP1 competition for CDI match predictions based on ITC measurements
 Predicted fraction of Ca_v1.2 channels bound to CaM as a function of [CaM]/[CaBP1] using values for the apo-state (black) and calcium-bound state (grey) IQ domain affinities measured by ITC (Table 1). Red diamonds show the fraction of CaM:Ca_v1.2 estimated from CDI measurements at varying ratios of injected CaM and CaBP1 protein. Teal curves show the prediction fraction of CaM-bound channels assuming that the K_d ratios of CaBP1/CaM apo-states differ from the measured values by a factor of 2 in favor of CaBP, (Δ2) CaBP1, or CaM, (Δ2) CaM. Orange curves are calculated assuming that the K_d ratios of CaBP1/CaM apo-states differ from the measured values by a factor of 10 in favor of CaBP, (Δ10) CaBP1, or CaM, (Δ10) CaM.

Table 1
Titration calorimetry data for interactions between CaM and CaBP1 with the Cav1.2 IQ domain

	n	Setup	N	K _d (M)	H (kcal mol ⁻¹)	S (cal mol ⁻¹ K ⁻¹)	G (kcal mol ⁻¹)	K _d CaBP1 / K _d CaM	K _d (apo) / K _d (Ca ²⁺)	G (kcal mol ⁻¹)
N-lobe _{BP} **	3	S	0.82 ± 0.05	1.10 × 10 ⁻⁶ ± 8.0 × 10 ⁻⁸	2.09 ± 0.40	34.5 ± 1.5	-7.84 ± 0.04	-	-	-
Ca ²⁺ /C-lobe _{BP} **	4	S	0.90 ± 0.07	1.05 × 10 ⁻⁸ ± 1.9 × 10 ⁻⁹	-2.88 ± 0.19	25.5 ± 0.6	-10.52 ± 0.11	-	-	-
Ca ²⁺ /CaBP1**	2	D	#	2.9 × 10 ⁻¹⁰ ± 7.0 × 10 ⁻¹¹	-4.72 ± 0.07	26.6 ± 0.7	-12.38 ± 0.14	-	-	-
Ca ²⁺ /N-lobe _{CaM} *	2	S	0.85 ± 0.05	5.76 × 10 ⁻⁸ ± 3.55 × 10 ⁻⁸	-1.91 ± 0.14	26.7 ± 0.9	-9.60 ± 0.38	19	-	-
Ca ²⁺ /C-lobe _{CaM} *	2	S	0.98 ± 0.18	2.63 × 10 ⁻⁹ ± 7.0 × 10 ⁻¹¹	-6.77 ± 0.21	14.2 ± 0.9	-11.31 ± 0.01	4.0	-	-
Ca ²⁺ /CaM	2	D	#	8.5 × 10 ⁻¹³ ± 1.3 × 10 ⁻¹³	-5.74 ± 0.35	34.5 ± 0.9	-15.68 ± 0.08	340	-	-
N-lobe _{BP} **	3	S	0.82 ± 0.05	1.10 × 10 ⁻⁶ ± 8.0 × 10 ⁻⁸	2.09 ± 0.40	34.5 ± 1.5	-7.84 ± 0.04	-	1	0
C-lobe _{CaBP1} EF34	2	D	#	3.80 × 10 ⁻⁶ ± 1.30 × 10 ⁻⁶	3.77 ± 0.20	37.7 ± 1.4	-7.08 ± 0.21	-	360	-3.44
CaBP1EF34	2	D	#	9.1 × 10 ⁻⁸ ± 1.3 × 10 ⁻⁸	-0.82 ± 0.15	29.0 ± 0.2	-9.15 ± 0.08	-	310	-3.24
N-lobe _{CaM} EF12	2	D	#	> 5 × 10 ⁻⁶	n/a	n/a	> -6.9	< 0.2	> 90	< -2.78
C-lobe _{CaM} EF34	2	D	#	2.2 × 10 ⁻⁶ ± 1.0 × 10 ⁻⁸	-3.79 ± 0.06	12.4 ± 0.2	-7.34 ± 0.02	1.7	840	-4.05
CaMEF1234	2	D	#	5.8 × 10 ⁻⁷ ± 5.0 × 10 ⁻⁸	-3.36 ± 0.02	16.5 ± 0.2	-8.10 ± 0.06	0.14	680,000	-7.58

G = RTln (K_d(apo) / K_d (Ca²⁺)), where T = 288K

** denotes data from ref. 30

*** denotes data from ref. 23

denotes that N was set to 1

S denotes a simple and D a displacement titration

n denotes the number of independent experiments.

n/a means not applicable

Table 2
Titration calorimetry data for interactions between CaM and CaBP1 with Cav1.2 IQ domain TripleA

	n	Setup	N	K _d (M)	H (kcal mol ⁻¹)	S (cal mol ⁻¹ K ⁻¹)	G (kcal mol ⁻¹)	K _{dIQAAA} / K _{dIQ}	G (kcal mol ⁻¹)
N-lobe _{CaBP1}	2	S	n/a	> 5 × 10 ⁻⁶	n/a	n/a	> -6.9	> 4.5	< -0.9
Ca ²⁺ /C-lobe _{CaBP1}	2	S	0.93 ± 0.01	2.21 × 10 ⁻⁷ ± 1.4 × 10 ⁻⁸	-1.45 ± 0.14	25.5 ± 0.6	-8.65 ± 0.03	21	-1.87
Ca ²⁺ /CaBP1	2	S	0.89 ± 0.19	1.09 × 10 ⁻⁸ ± 2.0 × 10 ⁻⁹	-4.77 ± 1.04	19.4 ± 4.0	-10.35 ± 0.11	38	-2.03
Ca ²⁺ /N-lobe _{CaM}	2	S	n/a	> 5 × 10 ⁻⁶	n/a	n/a	> -6.9	> 90	< -2.7
Ca ²⁺ /C-lobe _{CaM}	2	S	0.90 ± 0.01	1.54 × 10 ⁻⁹ ± 2.1 × 10 ⁻¹⁰	-6.44 ± 0.13	18.0 ± 0.1	-11.45 ± 0.08	0.6	0.14
Ca ²⁺ /CaM	2	D	#	1.7 × 10 ⁻¹⁰ ± 2.0 × 10 ⁻¹¹	-10.6 ± 0.4	7.4 ± 1.6	-12.68 ± 0.07	200	-3.00

G = RTln (K_{dIQAAA} / K_{dIQ}), where T = 288K

"#" indicates that N was set to 1.

"S" denotes a simple and "D" a displacement titration

"n" indicates the number of independent experiments.

"n/a" means not applicable.